

Graphdiyne: A Rising Star of Electrocatalyst Support for Energy Conversion

Bisheng Li, Cui Lai,* Mingming Zhang, Guangming Zeng,* Shiyu Liu, Danlian Huang, Lei Qin, Xigui Liu, Huan Yi, Fuhang Xu, Ning An, and Liang Chen

Graphdiyne (GDY), a rising star of 2D carbon allotropes with one-atom-thick planar layers, has achieved the coexistence of sp - and sp^2 -hybridized carbon atoms in a 2D planar structure. In contrast to the prevailing carbon allotropes, GDY possesses Dirac cone structures, which endow it with unique chemical and physical properties, including an adjustable inherent bandgap, high-speed charge carrier transfer efficiency, and excellent conductivity. Additionally, GDY also displays great potential in photocatalysis, rechargeable batteries, solar cells, detectors, and especially electrocatalysis. In this work, various GDY-supported electrocatalysts are described and the reasons why GDY can act as a novel support are analyzed from the perspective of molecular structure, electronic properties, mechanical properties, and stability. The various electrochemical applications of GDY-supported electrocatalysts in energy conversion such as hydrogen evolution reaction, oxygen evolution reaction, oxygen reduction reaction, overall water splitting, and nitrogen reduction reaction are reviewed. The challenges facing GDY and GDY-based materials in future research are also outlined. This review aims at providing an in-depth understanding of GDY and promoting the development and application of this novel carbon material.

1. Introduction


The vigorous exploitation of fossil fuels has made great contributions to the development of economy since the industrial revolution. Unfortunately, the conventional fossil fuels are depleted in large quantities with the ever-increasing energy demand, which has caused the global disquiet related to energy dilemma. In addition, the massive combustion of fossil fuels also brings

severe environmental disruptions such as global warming and particulate-matter pollution.^[1] It is worth noting that carbon dioxide in the atmosphere is growing year by year and its content now is approximate twofold larger than that before industrial revolution.^[2] Consequently, it is urgent to develop economical, high-performance, and environmentally benign technologies for energy conversion in response to the increasing global energy supply and environment deterioration.^[3] Among these technologies, electrocatalysis shows great potential in energy conversion.^[4] In this technology, electrocatalyst is the most critical component. Therefore, developing earth-plentiful, high-performance, and strongly stable electrocatalysts becomes a fundamental challenge. In recent year, tremendous efforts have been devoted to exploring suitable electrocatalysts and some alternatives have been successfully developed, including noble metals,^[5] transition-metal dichalcogenides,^[6] layered

double hydroxides,^[7] and single-atom catalysts.^[8] However, these developed novel electrocatalysts suffer from some drawbacks such as poor conductivity, low active sites, sluggish charge transfer, and severe agglomeration, which have negative effect on electrocatalytic performance. Previous study has confirmed that finding suitable substances to support these materials could be a good choice to offset these drawbacks.^[9] Carbon materials such as graphene,^[10] carbon nanofibers,^[11] carbon nanotubes,^[12] and carbon black^[13] have been widely employed as support for various electrocatalysts to enhance their catalytic performance and significant improvements have been obtained.

Notably, the above-mentioned carbon materials are all composed by one hybridized state carbon atom (sp^2 hybridization), while previous work has revealed that the presence of ethynyl units (sp hybridization) in carbon materials can bring diverse properties.^[14] Then a pondered question is proposed: can two different hybridized carbon atoms (sp and sp^2) coexist in one carbon material? In the late 1980s, Baughman et al. first predicted that the novel carbon allotropes of graphynes (GYs) contained two hybridized state carbon atoms, the sp - and sp^2 -hybridized states were separately originated from ethynyl units and aromatic moiety rings.^[15] Since then, tremendous efforts have been devoted to investigating the potential mechanical,

Dr. B. Li, Prof. C. Lai, M. Zhang, Prof. G. Zeng, Dr. S. Liu, Prof. D. Huang, Dr. L. Qin, Dr. X. Liu, Dr. H. Yi, F. Xu, N. An
College of Environmental Science and Engineering
Hunan University
Key Laboratory of Environmental Biology and Pollution Control
(Hunan University)
Ministry of Education
Lushan South Road, Changsha 410082, P. R. China
E-mail: laicui@hnu.edu.cn; zgming@hnu.edu.cn
Prof. L. Chen
Faculty of Life Science and Technology
Central South University of Forestry and Technology
Shaoshan Road, Changsha 410004, China

 The ORCID identification number(s) for the author(s) of this article can be found under <https://doi.org/10.1002/aenm.202000177>.

DOI: 10.1002/aenm.202000177

optical, and electronic properties of GYs through theoretical calculations and practical experiments.^[16] The results show that the coexistence of sp- and sp²-hybridized carbon atoms in GYs makes it possess high degree π -conjugation, regular ordered pore structure, and tunable electronic structure.^[17] GYs are authenticated to possess Dirac cones structure, which is previously regarded as the distinctive structure only owned by graphene.^[18] Besides, GYs are confirmed to exhibit natural bandgap and high-speed charge carrier mobility. The electron and hole mobility in GYs can reach $10^5 \text{ cm}^2 \text{ V}^{-1} \text{ s}^{-1}$ under ambient temperature, which are comparable to that of graphene and single-wall carbon nanotubes.^[19] Furthermore, the mechanical property of GYs can be changed with different numbers of acetylenic linkages and various stacking arrangements.^[20,21]

In 2010, Li et al. first prepared graphdiyne (GDY) by in situ cross-coupling method,^[22] which aroused great interest of chemists, physicists, material scientists and other researchers. Afterward, GDY was extensively applied to various fields, including rechargeable battery,^[23,24] catalysis,^[25] solar cell,^[26] biomedicine,^[27] gas separation,^[28] and water remediation.^[29] Very recently, GDY has been widely employed as a support for electrocatalysts to enhance energy conversion efficiency, including hydrogen evolution reaction (HER), oxygen evolution reaction (OER), oxygen reduction reaction (ORR), overall water splitting (OWS), and nitrogen reduction reaction (NRR). However, no related work has been done to thoroughly summarize these aspects. In this review, we first analyze why GDY can act as excellent support from structures and properties, then various GDY-supported electrocatalysts are reviewed and the roles of GDY in these hybrid materials are highlighted. In addition, the electrochemical applications of GDY-supported electrocatalysts in energy conversion are also summarized. Finally, the challenges and opportunities of GDY and GDY-based materials are also proposed based on our understanding to promote the further development of GDY.

2. Structure and Property

2.1. Molecular Structure

GYs are a class of 2D carbon allotropes, which are constituted by different numbers of benzene rings and acetylenic linkages ($-\text{C}\equiv\text{C}-$). This can lead to the formation of monatomic layer thickness of carbon network with sp- and sp²-cohybridized carbon atoms (**Figure 1a**).^[30] Because of sp and sp² cohybridization, four genres of carbon-carbon bonds exist in their structure: 1) $\text{C}_{\text{sp}^2}-\text{C}_{\text{sp}^2}$ bonds of benzene rings; 2) $\text{C}_{\text{sp}^2}-\text{C}_{\text{sp}}$ bonds between adjacent $\text{C}=\text{C}$ double bonds and $\text{C}\equiv\text{C}$ triple bonds; 3) $\text{C}_{\text{sp}}-\text{C}_{\text{sp}}$ triple carbon bonds; and 4) $\text{C}_{\text{sp}}-\text{C}_{\text{sp}}$ single carbon bonds between adjacent $\text{C}\equiv\text{C}$ bonds. Based on the number of acetylenic linkages between benzene rings, GYs can be named as graphyne (GY, one acetylenic linkage), GDY (two acetylenic linkages), graphytrine (GY-3, three acetylenic linkages), graphtetrayne (GY-4, four acetylenic linkages) and other allotropes (**Figure 1b–e**).^[31] The calculated equilibrium bond lengths of aromatic bonds, single bonds, and triple bonds are 1.40–1.50, 1.33–1.48, and 1.12–1.24 Å (**Table 1**), respectively.^[32] As for GDY, the bond lengths of $\text{C}_{\text{sp}^2}-\text{C}_{\text{sp}^2}$ (benzene ring)



Bisheng Li obtained his bachelor's degree from college of life and environmental science, Huangshan University, China, in 2016. He is currently in the second year of his Ph.D. in Hunan University under the supervision of Prof. Cui Lai. His current research interests include the synthesis of

electrocatalytic, photocatalytic, and photoelectrocatalytic nanomaterials and their application in energy conversion and environment purification.



Cui Lai graduated from the College of Environmental Science and Engineering of Hunan University in 2013 and received her Ph.D. degree in environmental science. She joined Professor Guangming Zeng's group at Hunan University after completing her Ph.D. degree. Her main research interests

are the development and environmental application of functional nanomaterials.



Guangming Zeng obtained his Ph.D. in 1988 from Wuhan University. He has been a professor and head of the College of Environmental Science and Engineering at Hunan University since 1996. His research interests include chemical biology, bioanalytical chemistry, bionanotechnology, and molecular engineering.

bonds, $\text{C}_{\text{sp}^2}-\text{C}_{\text{sp}}$ bonds (adjacent $\text{C}=\text{C}$ double and $\text{C}\equiv\text{C}$ triple bonds), triple $\text{C}_{\text{sp}}-\text{C}_{\text{sp}}$ bonds, and single $\text{C}_{\text{sp}}-\text{C}_{\text{sp}}$ bonds are calculated to be 1.41, 1.40, 1.24, and 1.33 Å, respectively.^[33] The multitudinous carbon-carbon bonds in GDY make it possess stronger structural flexibility compared to graphene, which is beneficial for synthesizing curved structures such as nanotubes. The crystal lattice parameters of GDY are optimally ascertained to be 9.38 Å for *a*, 9.38 Å for *b*, 3.63 Å for *c*, 120° for θ , and 3.7 Å for interlayer distance of GDY layers.^[34] Besides, because of the inferior coupling between aromatic ring moiety and alkynyl unit, the single bonds are dwindled and the aromatic bonds are elongated to characteristic values, which reveals the

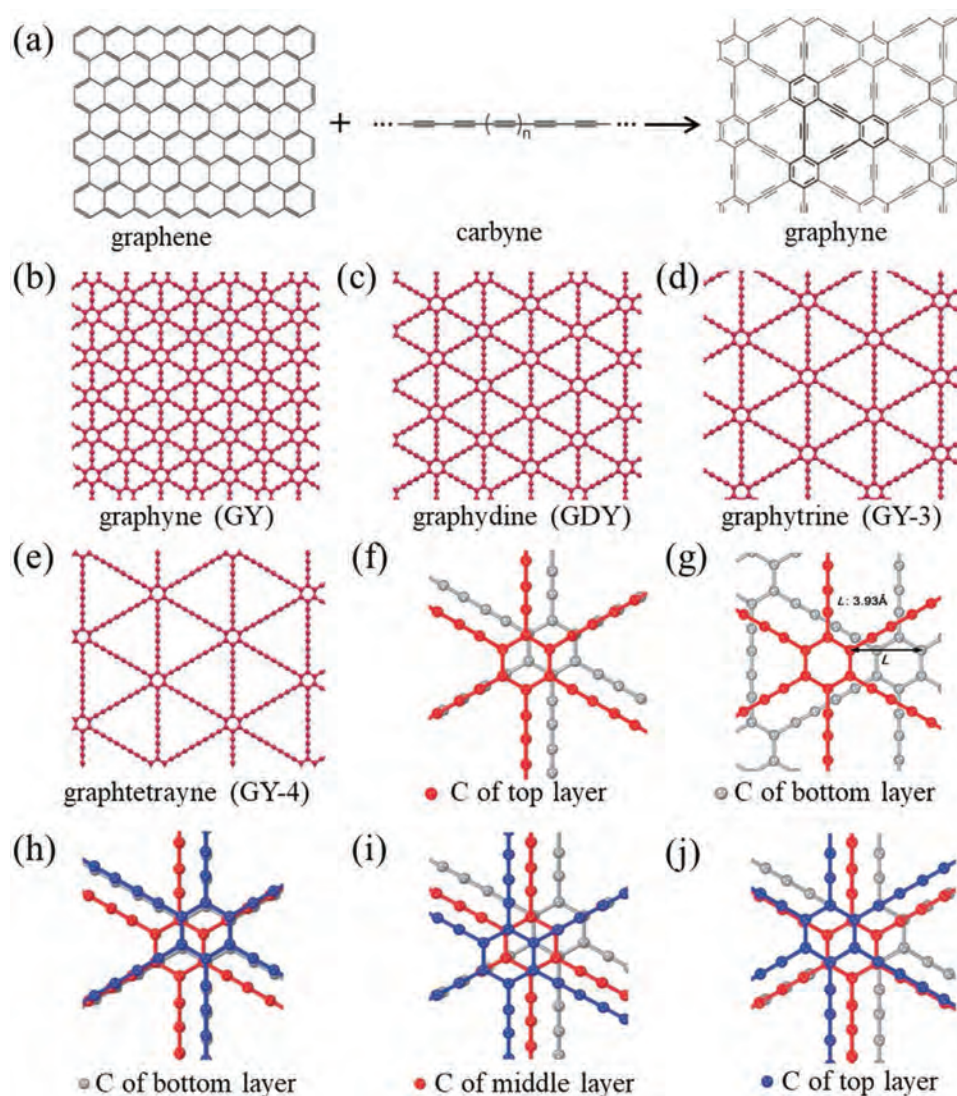


Figure 1. a) Schematic of graphene to GY-linking aromatic groups by linear acetylene. Reproduced with permission.^[30] Copyright 2013, Elsevier B.V. b–e) GYs with different numbers of acetylenic linkages. Reproduced with permission.^[31] Copyright 2019, Nature Publishing Group. Optimized configurations of bilayer GDY systems named AB (β_1) f) and AB (β_2) g) from top view; three possible configurations of the trilayer GDY systems from top view: h) ABA (γ_1), i) ABC (γ_2), and j) ABC (γ_3) configurations. Reproduced with permission.^[36] Copyright 2016, The Royal Society of Chemistry.

hybrid effect of sp - and sp^2 -hybridized carbon atoms. The lattice distances of GYs are quantitatively determined by average bond lengths. Previous work suggested that the lattice spacing had a homogeneous increase with the increasing content of acetylene linkage, the lattice spacing had an enhancement of 2.60 Å by adding one acetylene linkage.^[32] In addition, the quantum-level analysis also showed that one acetylene linkage could cause a lattice spacing enhancement of 2.58 Å. The single-layer 2D planar structure of GYs is stacked to form a layered structure by van der Waals force and π - π interaction. GYs have a regular 3D pore structure, and the triangular pores formed by benzene rings and acetylene bonds will lead to the formation of pores in layered GYs. In addition, GDY possesses high degree π -conjugation, regular ordered pore structure, and tunable electronic structure. These features make GDY exhibit great potentials in diverse domains, including catalysis, energy conversion,

energy storage, photoelectric conversion, biological application, and environmental remediation.^[35]

2.2. Electronic Properties

The electronic properties are critical factors for electrocatalytic materials, which can determine their various applications. Therefore, it is necessary to investigate the electronic properties of GYs to give an in-depth understanding of their instincts. The huge interest for GYs is ascribed to the never-before-seen electronic transport features. The first-principles calculations have declared that GYs allotropes possess the natural bandgap (inherent semiconducting characteristic), which is different from graphene with alleged gapless band structure. The bandgaps of GYs range from 0.46 to 1.22 eV, which depend on the

Table 1. Comparison of calculated equilibrium bond lengths (Å) Reproduced with permission.^[32] Copyright 2012, The Royal Society of Chemistry.

Work	Aromatic	Single	Triple	Note(s)
Here and Cranford and Buehler ^[20]	1.48–1.50	1.46–1.48	1.18–1.19	MD, ReaxFF potential; extended graphynes
Baughman et al. ^[15]	1.428	1.421	1.202	MNDO; canonical (1987); graphynes
Yang and Xu ^[37]	1.405–1.406	1.341–1.396	1.239–1.240	MD, REBO potential; extended graphynes ^{a)}
Narita et al. ^[38]	1.419	1.401	1.221	DFT, LSDA; extended graphynes
Bai et al. ^[39]	1.440	1.341–1.400	1.239	DFT, GGA-PBE; graphdiyne only ^{a)}
Mirnezhad et al. ^[40]	1.423	1.404	1.219	DFT, GGA-PBE; graphyne only
Peng et al. ^[41]	1.426	1.407	1.223	KS-DFT; graphyne only
Pei ^[42]	1.431	1.337–1.395	1.231	VASP, GGA-PBE; graphdiyne only ^{a)}

^{a)}Range in single bond length due to differentiation between interior single bonds (connecting two sp^1 carbons) and exterior single bonds (connecting sp^1 with sp^2 carbons). MD: molecular dynamics; MNDO: modified neglect of differential overlap; REBO: reactive empirical bond order; DFT: density functional calculations; LSDA: local-spin-density approximation; PBE: Perdew, Burke and Ernzerhof; GGA-PBE: generalized gradient approximation of Perdew–Burke–Ernzerhof; KS-DFT: Kohn–Sham density functional theory; VASP: Vienna ab initio simulation package.

applied technologies and exchange-correlation functions.^[43] For instance, Baughman's group declared that the bandgap of GDY was 0.79 eV through the extended Hückel level of theory.^[15] Lu's group reported that monolayer GDY possessed the bandgap of 1.10 eV based on GW many-body theory.^[44] Jiao's group pronounced that GDY owned a bandgap of 1.22 eV, which was very close to silicon (1.10 eV).^[45] In addition, the bandgap of GDY is extremely sensitive to strain, ribbon width, nanotube diameter, stacking mode, and applied electric field. Cui et al. stated that the bandgap of GDY raised from 0.47 to 1.39 eV with the increase of applied biaxial tensile strain, while decreased from 0.47 to near 0 eV with the increase of applied uniaxial tensile strain, which suggested that the applied strain could cause variation of GDY's electronic structure.^[46] In contrast to graphene nanoribbons, GY nanoribbons are semiconductors with a certain bandgap, and the bandgap reduces with the increase of the width.^[47] Interestingly, the electronic properties of GYs nanotubes change more greatly compared to common single-wall carbon nanotubes. Shohany et al. reported that the bandgaps of zigzag and armchair GDY nanotubes could be regulated by changing nanotubes diameter. Namely, the bandgap increased with the increase of nanotubes diameter. Meanwhile, zigzag GDY nanotubes possessed a smaller bandgap and higher diameter compared to armchair GDY nanotubes.^[48] As for bulk GDY, especially bilayer and trilayer GDY, the stacking mode also influences its electrical features. As displayed in Figure 1f,g, the stacking modes of AB (β_1) and AB (β_2) for double-layer GDY are the most stable configuration and second stable configuration.^[36] Meanwhile, the bandgaps of AB (β_1) and AB (β_2) are determined to be 0.35 and 0.14 eV. For trilaminar GDY, the stacking modes of ABA (γ_1), ABC (γ_2), and ABC (γ_3) possess the bandgaps of 0.32, 0.33, and 0.18 eV, respectively (Figure 1h–j).^[36] The above-mentioned results reveal that the bandgap of GDY is greatly relied on stacking mode. In addition, the bandgap is also affected by the applied electric field, the bandgaps of two-layer and three-layer GDY reduce with the enhancement of applied vertical electric field, regardless of stacking method.

A shocked discovery was reported that GY networks held extremely ultrahigh charge transport feature. That is to say, Dirac cones existed in GY networks, which was previously regarded as the distinctive feature of graphene because of the

hexagonal symmetry of graphene.^[49] In addition, this study also proclaimed that the Dirac points and cones not only existed in α -GY and β -GY with hexagonal symmetry, but also existed in 6,6,12-GY with rectangular symmetry. In other words, the presence of Dirac points and cones was not just determined by honeycomb structure or hexagonal symmetry. This work further investigated the electronic band structures of different types of GYs, result showed that the valence band and conduction band of α -GY and β -GY were intertwined at a point at Fermi level (0 eV) and situated at the identical location in the Brillouin zone, which were in line with the Dirac points of graphene. In addition, hexagonal symmetry blocks the significant direction-dependent electronic properties on these network planes. In contrast to graphene with hexagonal symmetry, 6,6,12-GY with rectangular symmetry displays four Dirac points in the Brillouin zone, which are divided into two pairs and these two pairs are originated from various carbon atomic orbitals. This result discloses the unconventional direction-dependent electronic properties such as novel conductivity. The hole and electron mobility in 6,6,12-GY are 4.3×10^5 and 5.4×10^5 $\text{cm}^2 \text{V}^{-1} \text{s}^{-1}$ under normal temperature, which are much larger than that of graphene (3.2×10^5 and 3.3×10^5 $\text{cm}^2 \text{V}^{-1} \text{s}^{-1}$). In addition, single-layer GDY also possesses excellent electron mobility of 2×10^5 $\text{cm}^2 \text{V}^{-1} \text{s}^{-1}$ under atmospheric temperature, its hole mobility is an order of magnitude lower than electron mobility.^[50] The superior charge carrier mobility makes it a promising support in electrochemical fields.

2.3. Mechanical Properties

Mechanical properties are also relatively appealing features for materials, especially for GYs. Previous study have reported that GDY possessed a lower in-plane Young's modulus of 162 N m^{-1} (53%) compared to graphene, revealing that it was softer than that of graphene.^[51] This is because the average coordination numbers of carbon atoms in GY networks are sparser than graphene, thereby leading to a smaller in-plane atomic mass density and electronic charge density. However, GDY displays a larger Poisson ratio of 0.429 compared to graphene and this value is almost equal to completely incompressible material,

which indicates that GDY volume can be well preserved under uniaxial strain. Cranfors and Buehler have employed ReaxFF MD to investigate the mechanical property of GYs. The result showed that GYs exhibited anisotropic feature and the scope of fracture strain for GYs was 8.2–13.2%, whereas the fracture stress range was 48.2–107.5 GP, which were comparable to that of graphene.^[20] The equilibrium interval between adjacent GYs layers is 3.20 Å, which is shorter than that of graphene (3.35 Å). This is ascribed to much looser configuration of carbon atoms in GYs, thereby leading to inferior surface energy landscape and making the equilibrium distance short. In contrast to graphene, the existence of looser carbon atoms configuration and directionality of acetylene linkages in GY networks make their internal stiffness rely on the applied load orientations, resulting in the nonlinear stress-strain behavior. Hou's group revealed that internal stiffness of GYs decreased from 75.6 to 12.3 N m⁻¹ when the number of acetylene linkages increased from 0 to 10, while the Poisson's ratio increased from 0.2 to 0.3.^[52] Yue's group also found that the internal stiffness had a downward trend for GY (166 N m⁻¹), GDY (123 N m⁻¹), GY-3 (102 N m⁻¹), and GY-4 (88 N m⁻¹) with the enhancement of acetylene linkages, and values of Poisson's ratio were 0.416, 0.446, 0.436, and 0.432, which only had a minor change. In addition, the incorporation of acetylene linkages caused the obvious reduction of stability, elastic modulus, and failure strength, and all of them were defined as a function of the number of acetylene linkages or the lattice spacing.^[53] In addition, Zhang et al. also discovered that the introduction of acetylene linkages in GYs had a great influence on Young's moduli, fracture strain, and fracture stress.^[21] The fracture strain and final stress for various structures forcefully rely on the different types of applied loads and this phenomenon can be interpreted by the distinctive bond extension and atomic stress distribution among various conformations of acetylene groups. All of these confirm that GYs possess excellent mechanical properties and GYs can be used as support for various electrocatalysts.

2.4. Stability

The diversification of carbon-carbon bonds in GYs can bring about strong structural flexibility, while it also results in the drawbacks of crippled mechanical stiffness and attenuated chemical stability. GYs are predicted to hold low formation energy and high thermal stability, despite the fact that their formation energy is higher than that of graphite.^[54] The existence of acetylenic linkages in GYs will decrease their stability, which is dissimilar to graphene and other sp²-hybridized carbon materials. The stability of GYs is constantly reduced with the consecutive increase of acetylenic linkages.^[32] Besides, density functional theory tight-binding (DFT-TB) calculation is employed to explore the stability and structural properties of GYs, where the dissimilarity between GYs and graphene is clarified as δE (per carbon atom).^[55] In view of sp- and sp²-hybridized carbon atoms in GYs, the energies of GYs are anticipated on the basis of the number of acetylene linkages and hybridizations. The result shows that the stability of GYs depends on the number of acetylene linkages. Given all that, the stability

of GYs extremely relies on the ratio of sp- to sp²-hybridized carbon atoms. Baughman and Eckhardt first forecasted that GYs held a relatively high thermal stability of 12.4 kcal mol⁻¹ per carbon atom through modified-neglect-of-diatomic-overlap quantum chemical calculations.^[15] It is generally known that the Gibbs free energy is an important indicator to evaluate the stability of materials and smaller Gibbs free energy usually represents higher stability. Accordingly, the stability of GYs can compare with other materials through Gibbs free energy, especially carbon materials. Qiao and his co-workers determined the Gibbs free energy of GDY to be 0.803 eV,^[39] and the Gibbs free energies of some related carbon allotropes such as diamond, graphite, carbon nanotube, fullerene, and graphene were approximate -0.022, -0.008, 0.114, 0.364, and 1.037 eV, revealing that GDY was more unstable than most of above-mentioned carbon allotropes. Nevertheless, the infinitely extended 2D plane of GDY has a certain wrinkle shape in order to maintain the stability of structure, which is identical with graphene. Among all GYs, GDY is confirmed as the most stable carbon allotrope containing two acetylene linkages.^[56] Consequently, GDY has been extensively used for energy conversion.

3. GDY Supported Electrocatalysts for Energy Conversion

3.1. GDY as Support for Electrocatalysts

3.1.1. GDY as Support for Metal Oxides

Metal oxides are regarded as highly efficient electrocatalysts and have been widely applied to electrochemical energy conversion.^[57] In order to enhance its performance, metal oxides are usually prepared as various nanostructures such as 0D, 1D, 2D, and 3D hierarchical morphologies to enlarge specific surface area and expose more active sites.^[58] However, preparing metal oxides with different nanostructures significantly weakens their conductivity and structural stability.^[59] Fortunately, recent studies have revealed that carbon components and especially all-carbon materials are suitable candidates to promote catalytic performance and structural stability of metal oxides.^[60]

The newly developed 2D sp- and sp²-cohybridized carbon allotrope of GDY has aroused great interest in scientific research owing to its unique physicochemical properties.^[61,62] The theoretical arithmetic reveals that the presence of sp-hybridized carbon atoms and triangular cavities in 2D GDY conjugated network are beneficial for forming tight interfacial contact with active constituents, which has not been detected in preceding developed sp²- and sp³-hybridized carbon allotropes.^[23] This strong interactivity is attributed to the sp-hybridized-carbon-rich structure, which accelerates the electron transfer process and strengthens the stability of metal oxides in electrochemical energy conversion. Recently, Xue's group developed an efficient electrocatalyst of NiO-GDY using nickel carbonate hydroxide nanocubes as precursor.^[63] Transmission electron microscopy (TEM) result showed that substantial NiO particles were generated after the dehydration of nickel carbonate hydroxide nanocubes by annealing treatment, resulting in the porous structure

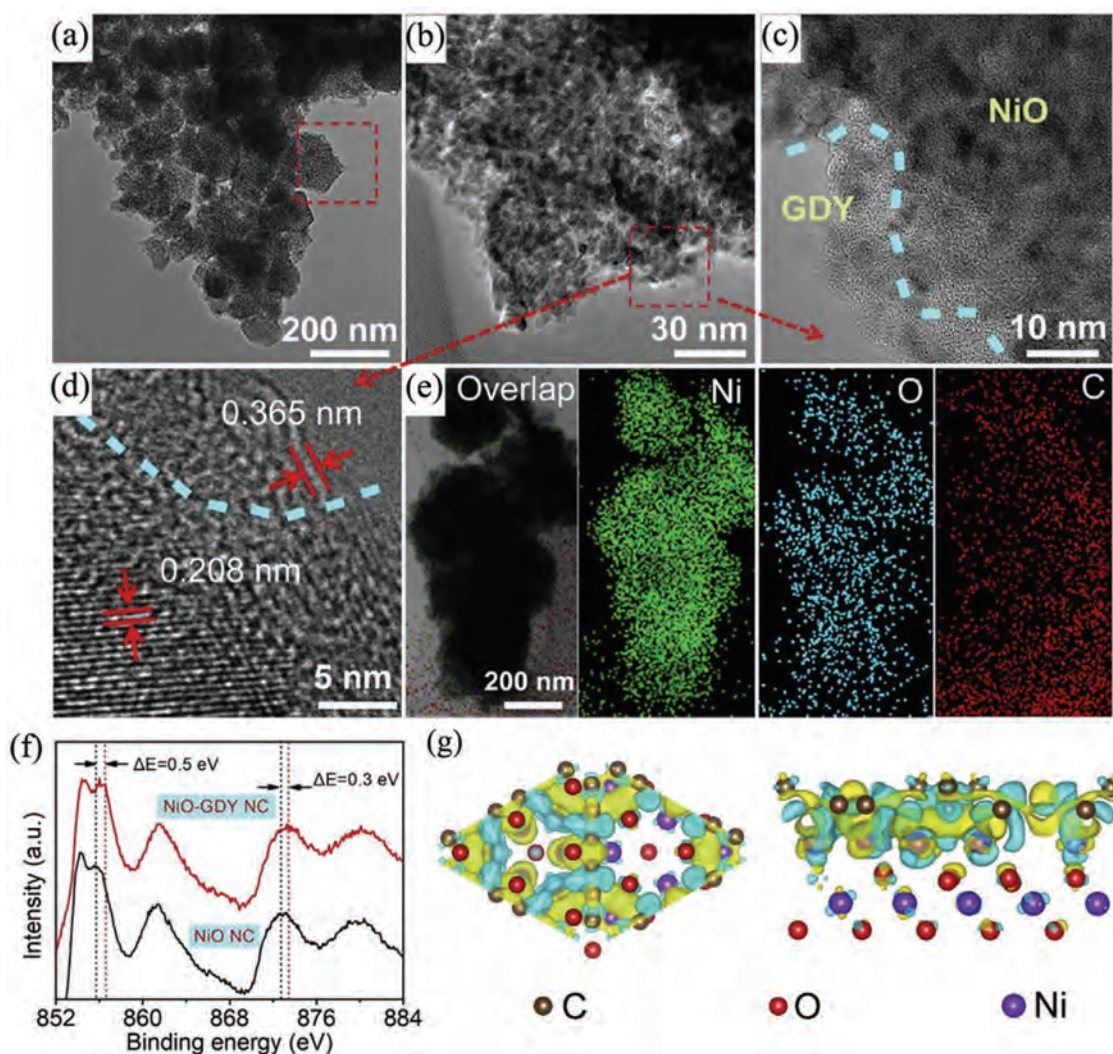


Figure 2. a) TEM and b–d) HRTEM images of NiO-GDY NC; e) EDX mappings of Ni, O and C in NiO-GDY NC nanocubes; f) comparison of high-resolution Ni 2p XPS spectra of NiO-GDY NC and pristine NiO NC (Figure 2f). This phenomenon revealed that electrons transferred from NiO to GDY, thereby promoting the conductivity of NiO. The DFT result also illustrated the palpable charge transfer between NiO and GDY, which was consistent with the result of XPS (Figure 2g). In addition, this electrocatalyst was prepared without using any binder, which also efficaciously lowered the resistance and enhanced the electrons transfer. Based on above-mentioned advantages, the prepared NiO-GDY electrocatalyst displayed superior performance for energy conversion.

of newly generated nanocubes (Figure 2a). The porous structure of prepared NiO-GDY not only enhanced the electrocatalytically active surface areas (EASAs), but also accelerated mass and ion transport. High-resolution transmission electron microscopy (HRTEM) and energy dispersive spectrometer (EDS) mapping indicated the successful preparation (Figure 2b–e). More importantly, the binding energies of Ni 2p_{1/2} and 2p_{3/2} of NiO-GDY had positive shift in X-ray photoelectron spectroscopy (XPS) spectra compared to pristine NiO (Figure 2f). This phenomenon revealed that electrons transferred from NiO to GDY, thereby promoting the conductivity of NiO. The DFT result also illustrated the palpable charge transfer between NiO and GDY, which was consistent with the result of XPS (Figure 2g). In addition, this electrocatalyst was prepared without using any binder, which also efficaciously lowered the resistance and enhanced the electrons transfer. Based on above-mentioned advantages, the prepared NiO-GDY electrocatalyst displayed superior performance for energy conversion.

3.1.2. GDY as Support for Transition-Metal Dichalcogenides

Up to now, precious-metal-based materials such as Pt, Ru, and Ir are proved to be high-performance electrocatalysts for electrochemical energy conversion, but the shortcomings of high cost, scarcity, and unsatisfactory stability make them unsuitable for commercialization.^[64] Many precious-metal-free electrocatalysts like phosphides,^[65] carbide,^[66] selenides,^[67] and transition-metal dichalcogenides (TMDs)^[68] have been developed to solve this problem. Among them, TMDs with inexpensive and resource-abundant features are potential alternatives. However, most of TMDs are still far from practical application because of their low catalytic activity and poor stability. Although uniting TMDs with various conductive carbon materials is deemed to be a method to accelerate electron transfer and obtain high performance,^[69] it still had a lot of room for further improvement.

Recently, Xue's group prepared a novel 3D flexible heterojunction material (eGDY/MoS₂) using electron-rich GDY

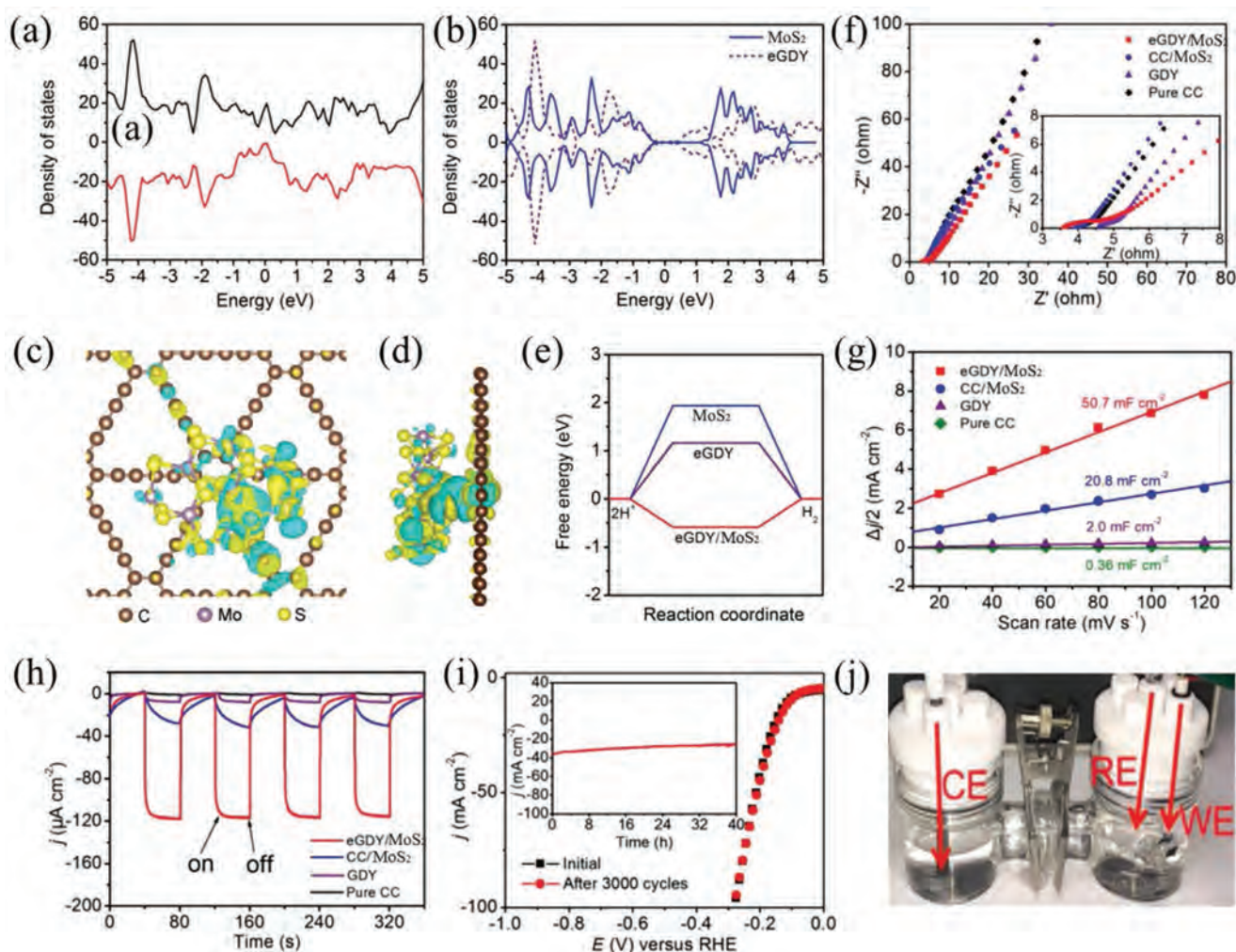


Figure 3. Density of states (DOS) of a) eGDY/MoS₂ and b) MoS₂ (blue line) and eGDY (dashed violet line), in which Fermi level is 0 eV; charge density difference maps for eGDY/MoS₂: c) top view and d) side view; e) hydrogen adsorption free energy (ΔG_H) on eGDY/MoS₂ (red line), eGDY (violet line), and MoS₂ (blue line); f) Nyquist plots of the catalysts in 0.5 M H₂SO₄; g) the capacitive currents at 0.70 V versus RHE plotted against the scan rates (20, 40, 60, 80, 100, and 120 mV s⁻¹) for eGDY/MoS₂, CC/MoS₂, GDY, and CC, respectively; h) transient photocurrent responses of the catalysts; i) polarization curves of eGDY/MoS₂ obtained before and after 3000 potential cycles (inset: time-dependent current density curve of eGDY/MoS₂ for 40 h); j) the electrolysis cell (two chambers) using eGDY/MoS₂ as cathode under working conditions (RE, the reference electrode; WE, the working electrode; CE, the counter electrode). Reproduced with permission.^[70] Copyright 2018, Wiley-VCH Verlag GmbH & Co. KGaA, Weinheim.

(eGDY) as support and MoS₂ as catalytic center, which was a superior catalyst for HER in both acid and alkaline conditions.^[70] DFT calculation showed that both pristine eGDY and MoS₂ possessed semiconductor property, while eGDY/MoS₂ hybrid material held metal conductor nature, which indicated the strong electronic interaction between eGDY and MoS₂ (Figure 3a,b). In addition, the hydrogen adsorption free energies (ΔG_H) of eGDY and MoS₂ were calculated to be 1.18 and 1.94 eV, revealing their stagnant property. However, the ΔG_H of eGDY/MoS₂ was -0.58 eV, revealing that it was more beneficial for hydrogen absorption and desorption (Figure 3c–e). Electrochemical impedance spectroscopy (EIS) was employed to estimate charge carrier transfer efficiency. The result showed that the solution resistance (R_s) and charge transfer resistance (R_{ct}) of eGDY/MoS₂ were 3.54 and 1.50 Ω in 0.5 M H₂SO₄ (3.67 and 5.20 Ω in 1.0 M KOH), which were much smaller than

that of pure carbon cloth (CC), CC/MoS₂, and pristine eGDY (Figure 3f). Besides, the electrical double-layer capacitance (C_{dl}) of eGDY/MoS₂ was 50.7 mF cm⁻², which was 2.44, 25.35, and 140.83 times larger than that of CC/MoS₂, eGDY and CC, indicating that eGDY/MoS₂ possessed large EASAs and tremendous uncovered active sites (Figure 3g). Furthermore, eGDY/MoS₂ held higher transient photocurrent (116 μ A cm⁻²), which was also larger than that of CC/MoS₂, eGDY, and CC (Figure 3h). In addition, this hybrid material also held excellent stability (Figure 3i,j). All of these evidences indicated that using eGDY as support not only accelerated electron transfer kinetics, but also provided more active sites. Furthermore, the massive pores and open spaces in eGDY/MoS₂ heterostructure expedited mass transport and gas bubbles release. The synergistic effect made this 3D flexible eGDY/MoS₂ possess superior electrocatalytic performance at all pH value.

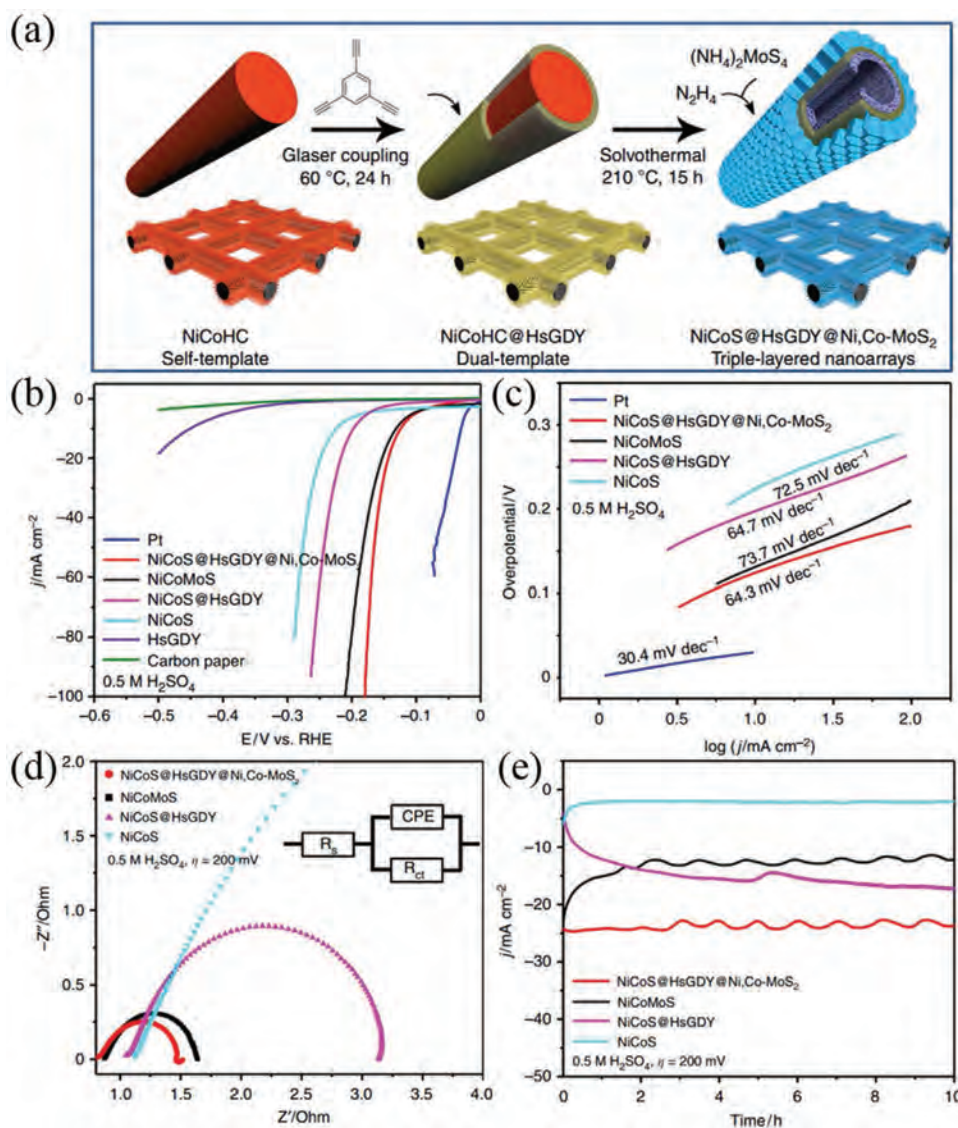


Figure 4. a) Schematic illustration of the fabrication of triple-layered nanotube arrays; b) HER polarization curves with iR compensations; c) Tafel plots; d) Nyquist plots derived from EIS, with an equivalent circuit (CPE (constant phase element), R_s (equivalent series resistance), R_{ct} (charge transfer resistance)); e) time-dependent current density curves without iR compensations of NiCoS@HsGDY@Ni,Co-MoS₂, NiCoMoS, NiCoS@HsGDY, NiCoS, HsGDY, Pt sheet, and carbon paper in 0.5 M H₂SO₄ (pH = 0.5). Reproduced with permission.^[71] Copyright 2018, Nature Publishing Group.

In 2018, Han and co-workers prepared a novel triple-layered sandwiched nanostructure using hydrogen-substituted GDY (HsGDY) frameworks as the middle layer, NiCoS (Co₉S₈/Ni₃S₂) as inner void, and Ni-Co co-doped MoS₂ (Ni,Co-MoS₂) as outer shell by dual-template synthetic method (Figure 4a).^[71] The middle layer of HsGDY not only worked as a separator to confine in situ transformation of nickel cobalt hydroxyl carbonate (NiCoHC) into NiCoS, but also acted as an ion channel to diffuse Ni²⁺ and Co²⁺ into outer layer to form Ni,Co-MoS₂. The proposed triple-layered nanostructure was anticipated to possess outstanding catalytic activity. To reveal the inherent catalytic activity of NiCoS@HsGDY@Ni,Co-MoS₂, iR (i denotes current and R denotes Ohmic electrolyte resistance) correction was employed to equalize the overpotential. As displayed in Figure 4b, NiCoS@HsGDY@Ni,Co-MoS₂

exhibited the best HER performance, the second was NiCoS@HsGDY and the worst was NiCoS, which indicated that each component in this sandwiched nanostructure played important role in catalytic process. Furthermore, NiCoS@HsGDY@Ni,Co-MoS₂ possessed the smallest overpotential of 124 mV with a Tafel slope of 64.3 mV decade⁻¹ at current density of 10 mA cm⁻², which was preferable to that of NiCoMoS (mixed Co₉S₈, Ni₃S₂, and Ni,Co-MoS₂), NiCoS@HsGDY, and NiCoS (Figure 4c). The HER behavior of NiCoS@HsGDY was better than that of NiCoS, which indicated that HsGDY was an important channel for electron and ion diffusion. In addition, the R_{ct} greatly reduced from 10 to 2 Ω after incorporating HsGDY with NiCoS, further confirming that HsGDY adjunction was better for electron transfer (Figure 4d).^[72] In addition, this sandwiched hybrid nanostructure held higher C_{dl} (75 mF cm⁻²), uncovering

that it owned larger EASAs and active sites. This sandwiched hybrid nanostructure also possessed high stability (Figure 4e). In brief, the incorporation of HsGDY made this triple-layered hybrid material possess distinctive built-in electron and ion channel, which was beneficial for the improvement of catalytic property.

Furthermore, Liu and co-workers developed layered WS₂/GDY 2D heterojunction using GDY as support to directly deposit WS₂.^[73] The Raman spectra exhibited that the intensity ratio of I_D/I_G was 1.06 for WS₂/GDY and it was much larger than that of pure GDY (0.74), indicating that more defects existed in WS₂/GDY heterojunction. This was because some S atoms were induced into GDY network during sulfurization treatment,^[74] which resulted in massive defects in WS₂. These defects could provide multitudinous reactive sites. In addition, the Fermi level of GDY was calculated to be −3.95 V based on ultraviolet photoelectron spectroscopy and the work function of WS₂ was 4.54 V, revealing that a Schottky barrier was generated at the interface between WS₂ and GDY. The presence of Schottky barrier indicated the fast charge transfer from GDY to WS₂, thereby boosting electrocatalytic activity. In 2018, Xue and his co-workers reported a creative heterojunction of MoS₂/NGDY (N-doped GDY) with outstanding catalytic performance.^[75] The outstanding catalytic performance was originated from three aspects: 1) the introduction of NGDY greatly reduced the aggregation of MoS₂, and thus enhancing EASAs and exposing numerous active sites; 2) the porous structure of NGDY in 3D MoS₂/NGDY heterojunction overwhelmingly promoted the mass transport; 3) the strong interactivity between MoS₂ and NGDY improved the electrical conductivity and heightened the charge migration efficiency.

3.1.3. GDY as Support for Transitional Metal Layered Double Hydroxides

Apart from TMDs, transitional metal layered double hydroxides (TM LDHs) are also desired candidates in the field of electrocatalysis owing to their distinctive features such as 2D laminated structure, adjustable chemical composition, and multifunctionalities.^[76] Nevertheless, low conductivity and poor stability are still two significant encumbrances of LDHs, which greatly weaken their catalytic behavior.^[77] Fixing LDHs on supports is deemed as an efficacious strategy to solve aforementioned encumbrances, and previous studies have successfully anchored LDHs on various substrates such as graphene,^[78] porous graphitized carbon,^[79] Ni₂P,^[80] NiCoP,^[81] and MXene,^[82] which obtained expected effect.

Recently, Xue's group successfully prepared a novel catalyst of GDY enwrapped Fe/Co layered double-hydroxide nanosheet arrays (Fe/Co-LDH@GDY/NF) through in situ growth strategy for OWS.^[83] The large interlayer distance and strong ion exchange ability of Fe/Co-LDH (ICLDH) gave the precursor of GDY access to its gallery, which was beneficial for generating GDY on ICLDH. At the same time, the stress/deformation caused by intimate contact between ICLDH and GDY enhanced interlamellar distance owing to its flexibility property, thereby leading to the entire exfoliation of bulk ICLDH (b-ICLDH) into few-layer ICLGH (e-ICLDH) and the generation of

2D/2D structure. This innovative strategy held three main superiorities compared to conventional electrocatalysts. First of all, the inherently strong electrical conductivity of GDY could overwhelmingly accelerate charge migration, thereby improving electrocatalytic performance; secondly, the massive triple bonds in GDY made it possess substantial charged carbon atoms and these charged carbon atoms worked as reactive sites. In addition, GDY was deemed as one of the most stable diacetylenic carbon allotropes,^[70,75] which could shield e-ICLDH from corroding and prolong its useful life. The theoretical studies showed that about 0.80e[−] migrated from ICLDH to GDY, confirming the intimate interaction between ICLDH and GDY (Figure 5a–d). Furthermore, the shift of binding energies in XPS and peaks in Raman spectrum also testified the electron migration (from e-ICLDH to GDY) (Figure 5e–g). The migrated electrons (from e-ICLDH to GDY in e-ICLDH@GDY) were favorable for the generation of *OOH specie with smaller free energy than that of pure GDY (0.54 vs 0.93 eV), thereby enhancing OER performance. In addition, the DFT calculation displayed that e-ICLDH@GDY was favorable for H₂O adsorption because the O 2p band of H₂O was overlapped with Fe 3d of e-ICLDH@GDY. e-ICLDH@GDY also displayed energetically favorable path with low adsorption (−0.56 eV) and preferable exothermal reaction heat for H₂ (−1.40 eV) (Figure 5h–j). More importantly, e-ICLDH@GDY also possessed the lowest transition state barrier of the intermediating H₂O splitting and the most energetically favorable chemisorption energy of HER (Figure 5k–m). Overall, e-ICLDH@GDY displayed excellent catalytic performance compared to pristine e-ICLDH and GDY, which would be a promising catalyst for OER and HER.

Wu's group first prepared superhydrophilic GDY (HGDY) through air–plasma treatment (the technology that usually enhances hydrophilic oxygenic groups of carbon materials) and then anchored ultrathin CoAl LDH on the surface of HGDY to form CoAl-LDH/HGDY hybrid material through electrostatic self-assembly method.^[84] The obtained CoAl-LDH/HGDY displayed unprecedented catalytic performance with a low overpotential of about 258 mV to attain 10 mA cm^{−2}, which was the best record for OER among all CoAl-based and GDY-based LDH electrocatalysts.^[85,86] The unprecedented catalytic performance was attributed to the electrostatic interaction between HGDY (negative charge density) and CoAl-LDH (positive charge density), which was favorable for catalyst combination. The high conductivity of HGDY accelerated the charge transfer and the superhydrophilic HGDY made catalyst have an intimate contact with electrolyte, thereby improving interfacial mass transport and electron transfer. In addition, other LDHs such as iron carbonate hydroxide nanosheets (FeCH),^[87] and nickel–iron layered double hydroxide (NiFe-LDH)^[88] were also successfully assembled on the surface of GDY. The prepared electrocatalysts showed outstanding catalytic activity, which confirmed that GDY was indeed an excellent support for LDHs.

3.1.4. GDY as Support for Metal Nitride

Apart from above-stated excellent electrocatalysts, transition-metal nitrides are also confirmed as outstanding catalysts

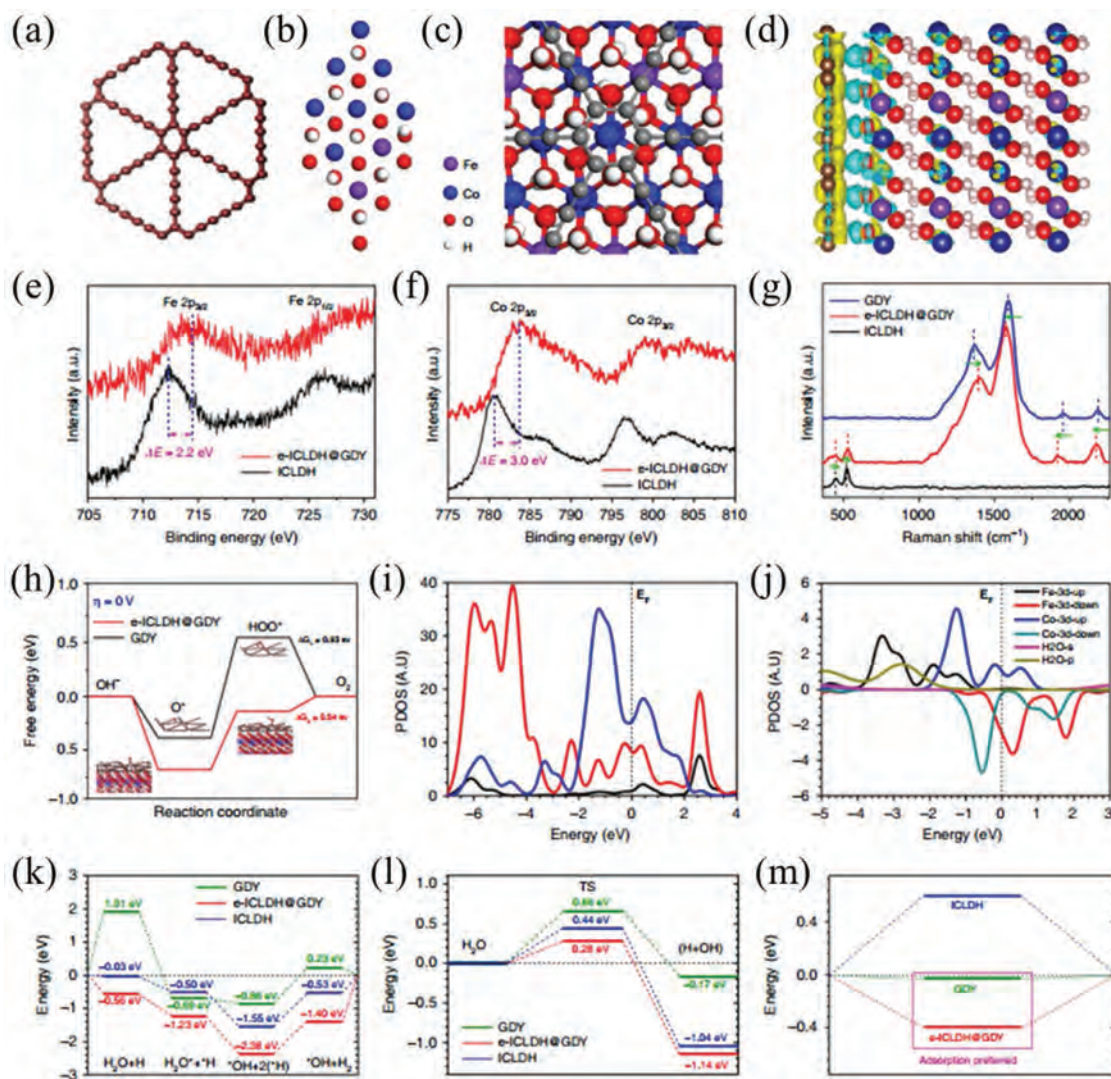


Figure 5. Theoretical calculations and structural analysis of the electrocatalysts. The stable configurations of a) GDY, b) ICLDH, and c) ICLDH@GDY; d) charge density difference for the stable configuration of ICLDH@GDY; e) Fe 2p and f) Co 2p core-level XPS spectra of the e-ICLDH@GDY/NF structure; g) Raman spectra of GDY, ICLDH, and e-ICLDH@GDY; arrows indicate the directions of the Raman spectral signals relative to those of e-ICLDH@GDY; h) the free energy changes for the formation of OOH* and corresponding stable structures of GDY (ΔG_1) and e-ICLDH@GDY (ΔG_2); i) PDOSs of the 3d and 2p bands of interfaced system containing GDY and ICLDH layers; j) PDOSs of Fe 3d, Co 3d, H₂O-s and H₂O-p bands near the interface region; k) Energetic pathway of HER under alkaline conditions for e-ICLDH@GDY, ICLDH, and GDY, respectively; l) Comparison on the transition state barrier for H₂O-splitting among three systems; m) H-chemisorption of these three systems. Reproduced with permission.^[83] Copyright 2018, Nature Publishing Group.

that have been applied to many fields as a result of their numerous active sites, robust stability, and low cost.^[89] Nevertheless, transition-metal nitrides also suffer from an identical shortcoming (low electrical conductivity) with metal oxide, TMDs, and TMLDHs, which renders their poor catalytic property.^[90] Hence, it is extremely important to strengthen their electrical conductivity, thereby boosting electrocatalytic performance.

In this respect, Xue and his co-workers assembled transition-metal nitrides with newly emerged planar carbon network of GDY (CoN_x@GDY) through a three-step strategy to enhance conductivity and energy conversion efficiency.^[91] A series of electrochemical characterization methods were

conducted to thoroughly discern the high electrocatalytic performance of hybrid material. EIS results showed that CoN_x@GDY exhibited the smallest semidiameter compared to pure CoN_x and GDY, indicating the smallest electric resistance (4.74 Ω) and highest charge transfer efficiency.^[92] In addition, the result of EASAs measurement showed that CoN_x@GDY also possessed a larger C_{dl} value (4.88 mF cm⁻²) than that of pristine CoN_x (3.45 mF cm⁻²), suggesting that CoN_x@GDY held much more active sites than that of pure CoN_x. Based on above-stated results, the incorporation of GDY not only increased electrical conductivity, but also produced numerous active sites, which significantly enhanced electrocatalytic performances.

3.1.5. GDY as Support for Metal Nanoparticles

As we know, surface active sites play critical role in electrochemical reaction kinetics.^[93] Regulating the size of materials to enlarge highly dense surface reactive sites is an efficacious method to boost catalytic behavior.^[94] However, downsizing the size of catalysts will enhance their surface energy, which results in the rigorous aggregation of catalysts.^[95] Thence, hunting for suitable and impactful catalyst support to strengthen the dispersion of catalysts and simultaneously reinforce electron-transfer kinetics is a matter of great urgency. Carbon materials with high surface-to-volume ratio, predominant electroconductivity, and high endurance are better choices to support nanoparticles,^[96] while the limited cycle life of such materials is a great challenge.^[97]

Very recently, GDY consisted by sp- and sp²-hybridized carbon atoms has triggered huge interest. Owing to the following unique properties, GDY would be an ideal support for metal nanoparticles. 1) The strong interaction between metal nanoparticles and alkyne or aryl π -conjugated network prevents nanoparticles from aggregation; 2) the presence of distinctive vesicular structure in GDY permits metal nanoparticles to embed with higher adsorption energy than that of graphene;^[98] 3) the superior electroconductivity is strong guarantee for making it an outstanding catalyst support. In 2016, Yang and co-workers developed a scalable and inexpensive way to fabricate GDY-supported Co nanoparticles (NPs) wrapped by N-doped carbon (CoNC/GDY) as an excellent electrocatalyst for HER.^[97] Previous study reported that the strong chemical adsorption between transition metals (such as Co) and alkyne rings of GDY was beneficial for depositing Co NPs on GDY surface.^[99] In addition, this strong interaction resulted in the faster electron migration from Co NPs to GDY, which enriched the electron density of GDY and thereby boosted electrocatalytic performance. EIS measurement also showed that CoNC/GDY electrocatalyst possessed the smallest R_{ct} (27.49 Ω in alkaline environment, 31.5 Ω in acid environment, and 22.69 Ω in neutral media) compared to pristine GDY and NC/GDY, revealing its high charge-transfer kinetics.^[100] Apart from above-mentioned superiorities, this electrocatalyst also possessed other advantages. On the one hand, the strong electrochemical conductivity of GDY made this electrocatalyst a highly conductive supporting matrix. On the other hand, the high porosity of GDY greatly expedited mass transfer and maximized the utilization of reactive sites. More importantly, Co NCs can be prevented from corrosion and aggregation by confining Co NCs into composite, and thus promoting the stability.

In 2017, Zhang and his co-workers used GDY as substrate to fasten cobalt nanoparticle to prepare a novel 3D Cu@GDY/Co electrocatalyst for oxygen evolution.^[101] The electrocatalytic performance test revealed that pure Cu foam did not generate anodic current within 1.6 V, and no considerable change on catalytic performance was observed when GDY grew on Cu foam, indicating that bare GDY did not possess catalytic property. However, when anchoring Co nanoparticle on Cu@GDY foam by in situ chemical reduction method, Cu@GDY/Co foam displayed higher anodic current than that of aforementioned materials with an onset potential of about 1.53 V. More importantly, the current density of 10 A m⁻² can be obtained

when only a low potential of approximate 1.65 V was applied. Unfortunately, there was no improved activity can be detected when only Co nanoparticles were fixed on Cu foam. In addition, inductively coupled plasma mass spectrometry (ICP-MS) result showed that only 0.6 $\mu\text{g cm}^{-2}$ of Co was adhered to pristine Cu foam. However, about 8.2 $\mu\text{g cm}^{-2}$ of Co could be attached to Cu@GDY, which was 13.7 times larger than that of pristine Cu foam, revealing that GDY was beneficial for Co nanoparticles stabilization. The Tafel plots and EIS suggested that Cu@GDY/Co foam possessed the smallest Tafel slope and radius among other electrodes, confirming the highest conductivity and the most excellent catalytic performance of Cu@GDY/Co foam. The obtained catalytic performance was equal to or even slightly better than that of other Co NPs-based catalysts reported in previous studies.^[102] The excellent catalytic activity was ascribed to the synergistic reaction of 3D Cu foam, GDY, and Co nanoparticles. Cu foam was used a 3D skeleton to prepare GDY, Co nanoparticles provided numerous active sites, and GDY was used as the support for Co nanoparticles to improve dispersion and simultaneously work as a channel for mass transport and electrons transfer.

3.1.6. GDY as Support for Single Atoms Catalyst

As mentioned above, downsizing the catalyst particle can expose more active sites. Therefore, regulating the size of catalyst to atomic scale (single atoms) will maximally expose active sites.^[103] Unfortunately, the high surface energy of single atoms makes them unstable and they are more prone to aggregate compared to nanoparticles during the fabrication and catalytic process.^[104] In addition, the low electroconductivity, small loading, and poor tolerance also depress their catalytic activity. Thus, single atoms are usually anchored on appropriate substrates to improve their dispersion and electroconductivity. The sp (p_x - p_y π/π^* states) and sp² (p_z π/π^* state) hybridization coexisted in GDY structure reveals that the π/π^* orbitals can rotate in any direction perpendicular to $-\text{C}\equiv\text{C}-$ bonds.^[99] This unique nature is more suitable for the anchoring of single atoms, and thus leading to high-speed charge carrier migration between single atoms and GDY. In addition, the valence states of previous reported single atoms were positive valence states^[105] or mixed valence states,^[106] while the zero-valence single atoms (only contain zero valence, also called as zero-valence metal atoms) have not been prepared. Fortunately, some zero-valence metal atoms have been prepared using GDY as support in recent year, which is regarded as a great breakthrough in the field of catalysis. Therefore, this section is divided into two parts, one is GDY-based traditional single atoms catalyst and another is GDY-based zero-valence metal atoms catalyst.

GDY-Based Traditional Single Atoms Catalyst: Last year, Lu and co-workers anchored single-atom Pt on GDY, and Pt atoms were homogeneous distributed on GDY via the coordination interaction between Pt atoms and alkynyl C atoms in GDY, in which Pt-GDY1 (GDY reacted with K₂PtCl₄ at 0 °C for 480 min) formed five-coordinated C₁-PtCl₄ species, while Pt-GDY2 (Pt-GDY1 annealed at 200 °C for 60 min under Ar condition) formed four-coordinated C₂-Pt-Cl₂ species.^[107] The

prepared Pt-GDY2 displayed amazing catalytic performance for HER, and the optimal catalytic performance was much superior than that of Pt-GDY1 and Pt/C electrocatalyst. A series of characterizations revealed that Pt-GDY2 possessed the highest total unoccupied density states of Pt 5d orbital compared to pristine GDY and Pt-GDY1. It is universally known that the vacant d orbitals of atomic catalysts play critical role in catalytic reaction, which commonly contributes to superior catalytic performance. This is because d orbital can interact with 1s orbital of H atom, which is favorable for transferring electron to H atoms.^[108] In addition, the computed Gibbs free energy of hydrogen adsorption (ΔG_{H^*}) showed that the ΔG_{H^*} of Pt-GDY2 was 0.092 eV. Compared to the ΔG_{H^*} of bare GDY (0.801 eV) and Pt-GDY1 (−0.653) eV, this value was similar with the ΔG_{H^*} of Pt metal (−0.09 eV).^[109] This result suggested that the excellent HER performance was also attributed to the topgallant ΔG_{H^*} for H adsorption on the per Pt active site. Therefore, the suitable ΔG_{H^*} and higher total unoccupied density states of Pt 5d orbital in Pt-GDY2 were in charge of the outstanding catalytic performance. In addition, GDY also was utilized as a suitable support for Sc/Ti single atoms^[110] and transition-metal single atoms,^[111] which greatly enhanced the high distribution of single atoms, accelerated electron transfer and promoted electrical conductivity, thereby boosting electrochemical energy conversion efficiency.

GDY-Based Zero-Valence Metal Atoms Catalyst: In 2018, Li and his coworker anchored zero-valence Ni⁰ and Fe⁰ atoms on GDY through electrochemical reduction method strategy.^[112] Subangstrom-resolution high-angle annular dark-field scanning transmission electron microscopy (HAADF-STEM) result showed that Ni and Fe atoms were evenly distributed on GDY and the sizes of them were about 1.23 and 1.02 Å, which were in line with the typical sizes of isolated Ni and Fe atoms. X-ray absorption near-edge structure (XANES) and extended X-ray absorption fine structure (EXAFS) spectra were utilized to further ensure that Ni and Fe were isolated atoms. The result displayed that only one peak (approximate 1.6 Å for Ni–C and 1.5 Å for Fe–C) existed in EXAFS spectra of Ni/GDY and Fe/GDY, while no other peaks (2–3 Å for Ni–Ni and 2.3 Å for Fe–Fe) were detected, which revealed that Ni and Fe were isolated atoms. In addition, XANES and EXAFS were further conducted for Ni/GDY and Fe/GDY after hydrogen reduction and result showed that XANES and EXAFS spectra remained unchanged, which indicated that Ni and Fe existed as metallic state in Ni/GDY and Fe/GDY. Furthermore, they also employed theoretical studies to confirm that only isolated Ni and Fe atoms existed in Ni/GDY and Fe/GDY system. Furthermore, there was a strong interaction and high-speed charge transfer between isolated Ni (Fe) atoms and GDY. The strong interaction between isolated Ni (Fe) atoms and GDY was favorable for stabilizing themselves on GDY surface. Meanwhile, the high-speed charge transfer from Ni (Fe) atoms to GDY was propitious to the promotion of electrical conductivity and electrocatalytic activity.

Very recently, Xue's group successfully stabilized zero-valence palladium atoms (Pd⁰) on GDY surface through electrochemical deposition, which displayed superior HER performance.^[113] The authors investigated the critical mechanism of superior HER performance through their proposed two-way crossover linear response technique.^[114] The result showed that both

singly and triply symmetrically fixed Pd atoms held the closed shell (crossover) effect, which manifested the formidable orbital overlaps between Pd atoms and adjacent C atoms. Moreover, the raised orbital energy indicated that electronegativity was enhanced, further revealing the suitable deposition of Pd⁰ on GDY surface. The projected partial density of states (PDOSs) showed that the bonding between Pd atom and C1 and C2 sites (carbon atoms near Pd atoms) in Pd Pd⁰/GDY system was much stronger than that in Ni-GDY system, indicating the high-speed charge transfer between Pd atoms and neighboring C sites.^[112] In addition, theoretical arithmetic disclosed that C1 and C2 sites were preferable for H adsorption, C3 and C4 sites (carbon atoms away from Pd atoms) were favorable for H desorption, and this result assured the excellent HER performance. The above-mentioned theoretical evaluation corroborated that GDY was an ideal support for Pd⁰ anchoring, and it was further verified by experiment. Scanning electron microscope (SEM) and TEM showed that GDY was formed as ultrathin nanosheet and intertwined with each other to form a vertically aligned film on Cu foam (Figure 6a–c). After anchoring Pd⁰ on GDY surface, the morphology did not change, revealing the robust feature of GDY skeleton (Figure 6e–g). HRTEM suggested that Pd⁰/GDY hybrid material had an interplanar spacing of 0.329 nm, which was smaller than that of pristine GDY. The distance between two neighbor GDY layers became smaller, indicating the strong interactivity between them (Figure 6d,h). In addition, Pd⁰ cannot be observed in SEM, TEM, and HRTEM, confirming the high dispersion of Pd⁰ on GDY surface. HAADF-STEM images discovered that Pd⁰ was uniformly distributed on the surface of GDY and no apparent aggregation was detected (Figure 6i–l). STEM images and elemental mapping images also confirmed the well-proportioned dispersion of the monatomic Pd atoms on GDY surface (Figure 6m–p).

Very recently, Li's group also prepared a novel GDY-supported zerovalent Mo atoms catalyst by one-step solvothermal reduction method.^[115] ICP-MS measurement showed that a high loading amount of zerovalent Mo atoms (7.5%) could be achieved by this method, which was much higher than that of previously reported single atoms catalysts.^[116] Various characterizations such as SEM, TEM, HRTEM, and XRD have testified that no Mo NPs formed and EDS mapping displayed the high dispersion of Mo atoms in Mo⁰/GDY. In addition, HAADF-STEM distinctly exhibited the isolated and well-distributed bright dots, which corresponded to heavy-element atoms on GDY surface and confirmed the successful preparation of Mo⁰/GDY. EXAFS spectra revealed that only one obvious peak at 1.2 Å appeared, which was in line with Mo–C interactions. However, no peak related to Mo–Mo bond can be observed in EXAFS spectra, certifying that Mo only existed as isolated Mo atoms. In addition, EXAFS spectrum of Mo⁰/GDY was identical with the EXAFS spectrum of Mo reference, and the pre-edge derivative of XANES of Mo⁰/GDY catalyst resembled metallic Mo, revealing the zerovalent Mo atoms. Furthermore, the top valence band of Mo⁰/GDY was near to Fermi level compared to pure GDY, indicating the high conductive capacity of Mo⁰/GDY. Besides, they employed PDOSs to investigate the exceptional electronic activity of Mo⁰/GDY. Results showed that the electron-transfer behavior was controlled by the Mo 4d and C-p orbitals and the Mo 4d bands were fixed in the middle crossover of the Fermi

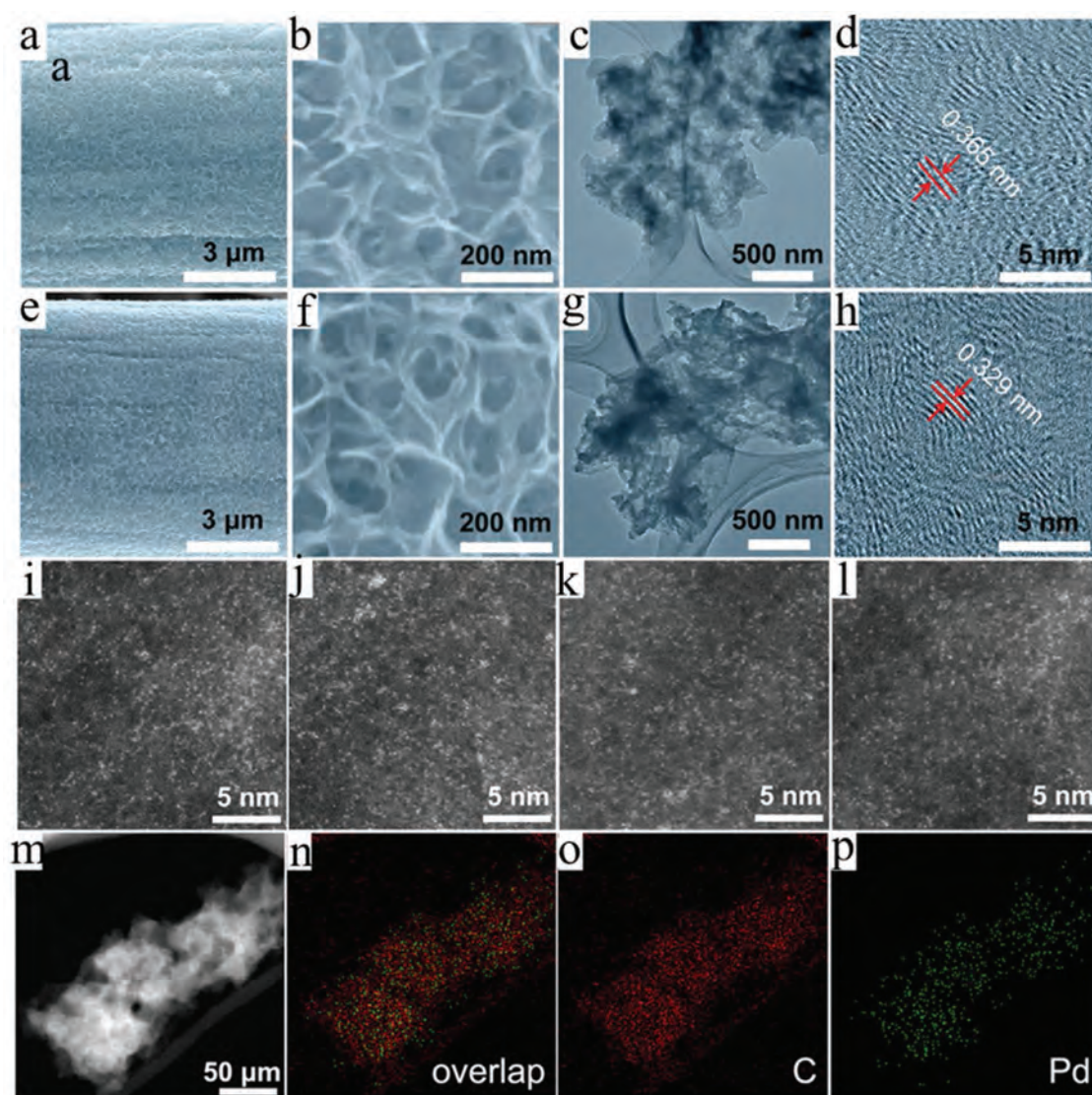


Figure 6. a,b) SEM, c) TEM, and d) HRTEM images of pristine GDY; e,f) SEM, g) TEM, and h) HRTEM images of Pd⁰/GDY; i–l) HAADF images obtained from various regions of Pd⁰/GDY nanosheets; m–p) STEM-HAADF image of the Pd⁰/GDY nanosheet and corresponding elemental mappings of Pd and C atoms. Reproduced with permission.^[113] Copyright 2019, Elsevier B.V.

level by two dominant C-bonding and antibonding orbitals. This result not only favored the preservation of Mo 4d valence electronic states for diverse electrocatalytic process, but also guaranteed that Mo sites could extract electron from C sites and then transfer to N sites. In short, the prepared Mo⁰/GDY electrocatalyst possessed excellent catalytic performance.

3.2. Applications

3.2.1. Hydrogen Evolution Reaction

With rapid consumption of conventional fossil fuel, the problems of energy shortage and environmental pollution are also coming. Developing a promising strategy to generate clean energy is a goal of world.^[117] Hydrogen is believed as a clean and sustainable energy and electrochemical splitting water is

considered to be a promising, efficacious, and benign tactic for hydrogen evolution.^[118] HER occurs at negative electrode in electrocatalytic hydrolysis process, which owns intrinsic superiority for providing hydrogen because of the enormous water resource.

Xue's group first utilized NGDY as stabilizer to anchor MoS₂ nanosheet on its surface for HER.^[75] The accelerated charge transfer, improved mass transport, and exposed reactive sites made it a superior electrocatalyst with high activity. The HER result showed that this MoS₂/NGDY catalyst only required a low overpotential of 186 mV to reach current of 10 mA cm⁻², which was superior to that of previous MoS₂-based electrocatalysts and even overmatched commercial Pt catalyst. Although MoS₂/NGDY possessed outstanding catalytic performance for HER, it still had a lot of room for improvement. Therefore, this group also fabricated a heterojunction using eGDY as support and MoS₂ as catalytic activity center in the same year.^[70] As expected, the prepared heterojunction showed wonderful

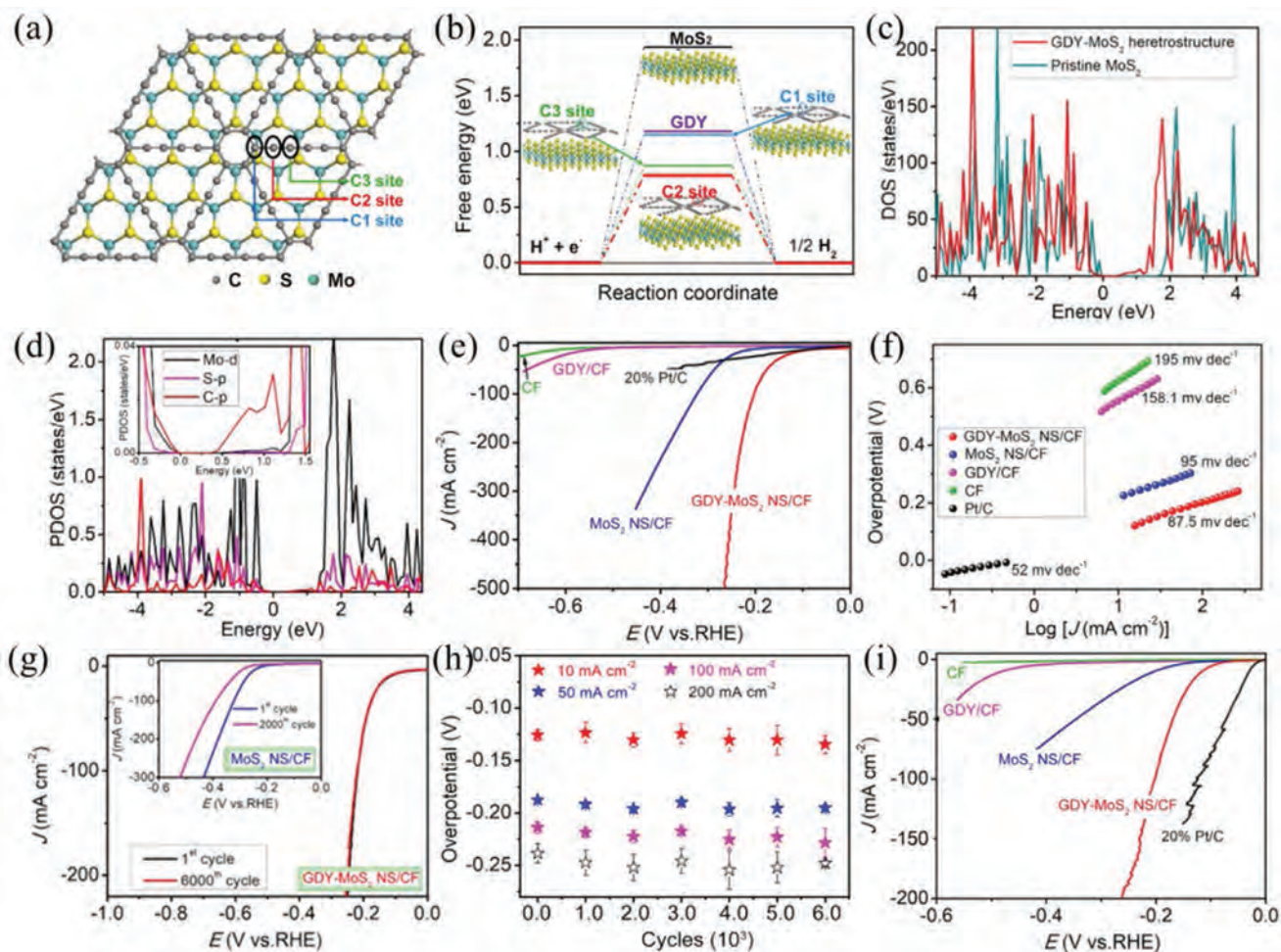


Figure 7. a) Top view of the optimized structures of GDY-MoS₂; b) Free-energy diagram of HER at equilibrium potential based on DFT calculation for pristine MoS₂, GDY and different sites in GDY-MoS₂ (blue line: C1 site; red line: C2 site; green line: C3 site). Insets: Optimized H-adsorption on different sites of GDY; c) DOS for pristine MoS₂ and GDY-MoS₂ heterostructure. d) PDOS (DOS on specified atoms and orbitals; Mo-d: d-orbital of Mo; S-p: p-orbital of S; C-p: p-orbital of C) for GDY-MoS₂ (Inset: the enlarged view of the marked region); e) Linear sweep voltammetry (LSV) curves; f) corresponding Tafel plots of as-synthesized electrocatalysts; g) LSV curves of GDY-MoS₂ NS/CF and MoS₂ NS/CF recorded before and after continuous cycling tests; h) The overpotentials at 10, 50, 100 and 200 mA cm⁻² after every 1000 cycles; i) LSV curves in 0.5 M H₂SO₄. Reproduced with permission.^[119] Copyright 2013, Elsevier B.V.

HER performance and the electrocatalytic HER measurement exhibited that eGDY/MoS₂ just needed an overpotential of 128 mV to obtain current density of 10 mA cm⁻² under acidic condition, which was better than that of eGDY, MoS₂, and previously reported MoS₂/NGDY electrocatalyst.^[75] In addition, He and his co-workers also fabricated GDY nanosheet coated MoS₂ nanosheet arrays grown on carbon fiber network (GDY-MoS₂ NS/CF) with the help of hydrothermal strategy and cross-coupling process.^[119] The obtained heterostructure catalyst displayed predominant HER performance under both acidic and alkaline condition. DFT result suggested that the introduction of GDY could overwhelmingly reduce the ΔG_H (from 1.94 to 0.78 eV) of MoS₂ (Figure 7a,b), benefiting for H adsorption (critical step in water splitting). In addition, PDOS showed that the presence of C 2p orbital lowered the conduction band minimum, indicating that the introduction of GDY decreased the bandgap and increased the electroconductivity (Figure 7c,d). The HER performance test showed that GDY-MoS₂ NS/CF

possessed the highest electrochemical performance with ultrahigh current density and ultralow overpotential in alkaline environment. GDY-MoS₂ NS/CF only demanded low overpotential of about 90 mV to realize current density of 10 mA cm⁻², which was 1.15, 2.42, and 6.78 times lower than that of 20% Pt/C, MoS₂ NS/CF and GDY/CF. This electrocatalytic performance was also more preferable than that of great majority of state-of-the-art catalysts (Figure 7e).^[120] In addition, GDY-MoS₂ NS/CF held the smallest Tafel slopes of 88 mV decade⁻¹ compared to pristine MoS₂ NS/CF and GDY/CF of 95 and 158 mV decade⁻¹ (Figure 7f). GDY-MoS₂ NS/CF also exhibited high durability without reduction of electrocatalytic performance after thousands of consecutive cycles (Figure 7g), and there was no difference of overpotential at 10, 50 and 100, and 200 mA cm⁻² after 1000 cycles, further confirming its high stability (Figure 7h). More importantly, GDY-MoS₂ NS/CF also owned superior HER performance compared to other catalysts (Figure 7i), suggesting its universality in both acidic and alkaline condition.

Furthermore, Wang's group developed a novel 3D Cu@GDY core-shell heterojunction through simple self-catalyzed growth route.^[121] The prepared Cu@GDY exhibited amazing HER activity, it acquired comparatively low overpotentials of 79 and 162 mV to reach catalytic current densities of 10 and 100 mA cm⁻². This HER performance was much better than that of previously reported non-precious-metal-based materials under acid condition.^[122] More importantly, the shell layer of GDY served as the chemically unanimated and mechanically stable platform to protect hybrid material from degrading, which was beneficial for enhancing its stability. Thus, this Cu@GDY core-shell material stayed the identical polarization curve after thousands of operations and even retained high catalytic performance for 20 h, discovering its strong stability. The unexpected HER performance and ultrahigh stability coupling with low-cost and large-scale fabrication procedure made it a potential candidate for practical energy conversion. Yang and co-workers reported an electrocatalyst of CoNC/GDY with high-performance for HER under all values of pH.^[97] This electrocatalyst also possessed strong stability, it could maintain high activity after successive 36 000, 38 000, and 9000 operations under alkaline, acidic, and neutral conditions, which was more excellent than that of 10% Pt/C catalyst under the completely same condition. Moreover, Liu and his co-workers reported a 2D/2D WS₂/GDY heterojunction electrocatalyst which synthesized by facile hydrothermal method.^[73] During the preparation process, some S atoms escaped from WS₂ and doped into GDY, thus resulting in numerous defects in WS₂. These defects could work as active edges. This 2D/2D structure also provided large specific surface area for catalytic reaction. In addition, a built-in electric field was also generated at the interface between WS₂ and GDY owing to the suitable energy band alignment, which enhanced the charge transfer between WS₂ and GDY. Therefore, this defect-rich 2D/2D structure held outstanding HER activity with decreased onset potential (140 mV) and low Tafel slope (54 mV decade⁻¹). Li and co-workers anchored zero-valence stable transition-metal atoms on the surface of GDY to investigate its electrocatalytic performance for HER.^[112] Surprisingly, this GDY-supported zero-valence isolated atom (Ni⁰ and Fe⁰) electrocatalyst displayed unprecedented electrocatalytic HER performance. Fe⁰/GDY displayed the highest HER performance with the smallest onset potential of 9 mV compared to pristine GDY and Ni⁰/GDY, and this HER activity was also comparable to that of Pt/C. Fe⁰/GDY and Ni⁰/GDY showed the overpotentials of 66 and 88 mV at 10 mA cm⁻², which overmatched other earth-rich electrocatalysts, even noble-metal-based electrocatalysts.^[123,124] In addition, the turnover frequency (TOF) values of Ni⁰/GDY and Fe⁰/GDY at 100 mV were 1.59 and 4.15 s⁻¹, which were also better than that of newly developed electrocatalysts, including CoP and Ni₂P (0.046 and 0.015 s⁻¹).^[108,123] Apart from excellent HER performance, Ni⁰/GDY and Fe⁰/GDY also exhibited strong durability, because they could stay high performance after successive 5000 cycles. Based on above-mentioned examples, GDY-supported electrocatalysts indeed possess high activity for HER and we believe that more and more GDY-based electrocatalysts will be developed for electrochemical energy conversion and other energy-related applications.

3.2.2. Oxygen Evolution Reaction

OER is believed as the key procedure of some electrochemically energy-related transformation and storage technologies, including water splitting,^[125] metal-air battery,^[126] and regenerative fuel cell.^[127] However, contrary to HER of cathode reaction, OER occurred in anode is generally subjected to sluggish kinetics owing to the multistep proton-coupled electron transfer process, which is the biggest obstacle in energy conversion and storage.^[128] Therefore, enhancing OER performance commonly needs to reduce the overpotential, expedite the kinetics, and strengthen the stability. Enormous endeavors have been devoted into this challenge and many excellent catalysts have been developed to meet this challenge.

In 2018, Yu and co-workers synthesized a new catalyst of GDY/NiFe-LDH using GDY as the promising support to promote the water oxidation ability through facile in situ growth method.^[88] DFT calculation revealed that the distance between GDY and NiFe-LDH was 0.206 nm, which was shorter than the distance between reduced oxide graphene (RGO) and NiFe-LDH (0.229 nm), suggesting a stronger chemical interaction between GDY and NiFe-LDH. Additionally, the adhesive energy of GDY/NiFe-LDH (-2.81 eV) was also more negative than that of RGO/NiFe-LDH, discovering its high stability. More importantly, the work function of GDY (5.13 eV) was higher than that of RGO (4.25 eV), signifying that transferring electrons from NiFe-LDH to GDY was more favorable. The aforementioned theoretical arithmetic announced that GDY/NiFe-LDH held much stronger chemical and electronic interaction compared to RGO/NiFe-LDH. Hence, the obtained GDY/NiFe-LDH hybrid material displayed outstanding OER performance and only a low overpotential of 260 mV was demanded to obtain catalytic current density of 10 mA cm⁻², which was the lowest value among RGO/NiFe-LDH (277 mV), CNT/NiFe-LDH (285 mV), NiFe-LDH (340 mV), and commercial RuO₂ (390 mV). GDY/NiFe-LDH nanocomposite also possessed the smallest Tafel slope (71 mV decade⁻¹) and highest TOF (0.025 s⁻¹) compared to RGO/NiFe-LDH (85 mV decade⁻¹, 0.019 s⁻¹), CNT/NiFe-LDH (97 mV decade⁻¹, 0.015 s⁻¹), and NiFe-LDH (169 mV decade⁻¹, 0.006 s⁻¹), guaranteeing its advantageous electrocatalytic kinetics and intrinsically high activity. In addition, chronopotentiometry test indicated no obvious reduction of inessential voltage could be detected after successive operations (10 000 s). Furthermore, the durability measurement of GDY/NiFe-LDH was also conducted under different current densities and higher overpotentials, the result showed that this hybrid material still maintained stable overpotentials under different applied current densities and stable current densities under higher overpotentials. All of these could testify the high durability of GDY/NiFe-LDH nanocomposite. The excellent catalytic performance, high durability, low cost, and mild preparation process rendered it with tremendous potentials in energy-related fields.

Recently, Zhang's group also designed and fabricated a novel metalloporphyrin-based GDY analogue (Co-PDY) through Glaser-Hay coupling reaction.^[129] The prepared Co-PDY owned broadened pore structure (2.34 nm), which could act as the fast transport channel for small molecules, benefiting for the improvement of catalytic kinetics. At the same time,

Co atoms in metalloporphyrin moieties structure supplied numerous catalytically active sites, and electrons migrated quickly through butadiyne linkages during catalytic reaction. Therefore, the obtained Co-PDY nanomaterial showed superior OER performance, which merely required a low overpotential of 270 mV to attain current density of 10 mA cm⁻². Meanwhile, this Co-PDY nanomaterial also possessed small Tafel slope of 99 mV decade⁻¹ and ultrahigh stability. Except for above-mentioned catalysts, other GDY-based materials have been successfully developed for OER and exhibited amazing catalytic performance.^[86,130]

3.2.3. Oxygen Reduction Reaction

Fuel cell, one of devices that directly converts chemical energy into electric energy, has been regarded as a promising technology to provide clean and sustainable energy for future.^[131] However, this promising technology suffers from two great bottlenecks of low energy conversion efficiency and poor stability, which significantly prevent it from practical application (commercialization).^[132] These bottlenecks mainly

originate from the essentially poor kinetics of ORR and the low durability in acidic or alkaline electrolyte.^[133] Accordingly, more energy should be devoted to exploiting high-performance catalyst to accelerate ORR kinetics and strengthen stability, thereby enhancing the whole energy conversion efficiency of fuel cell.

In 2018, Wu and his co-workers proposed a novel electrocatalyst of GDY-fastened single atomic level Fe atoms (Fe-GDY) by facile NaBH₄ reduction method. DFT calculation and experimental validation verified that Fe-GDY was a remarkable electrocatalyst for ORR.^[134] The adsorption energy computation indicated that the fastened Fe atoms served as reactive sites and strongly interacted with ORR intermediate products rather than carbon atoms with sp² hybridization in C6 ring or sp-hybridized carbon atoms in acetylenic-like rods because of its large spin and high positive charge (**Figure 8a**). In addition, the free energy calculation was also conducted to theoretically estimate ORR performance of Fe-GDY under equilibrium potential and applied certain overpotential. Result revealed that the free energy of Fe-GDY for rate-determining-step was much smaller than that of Pt (111) catalyst, suggesting that Fe-GDY possessed higher ORR performance compared to Pt

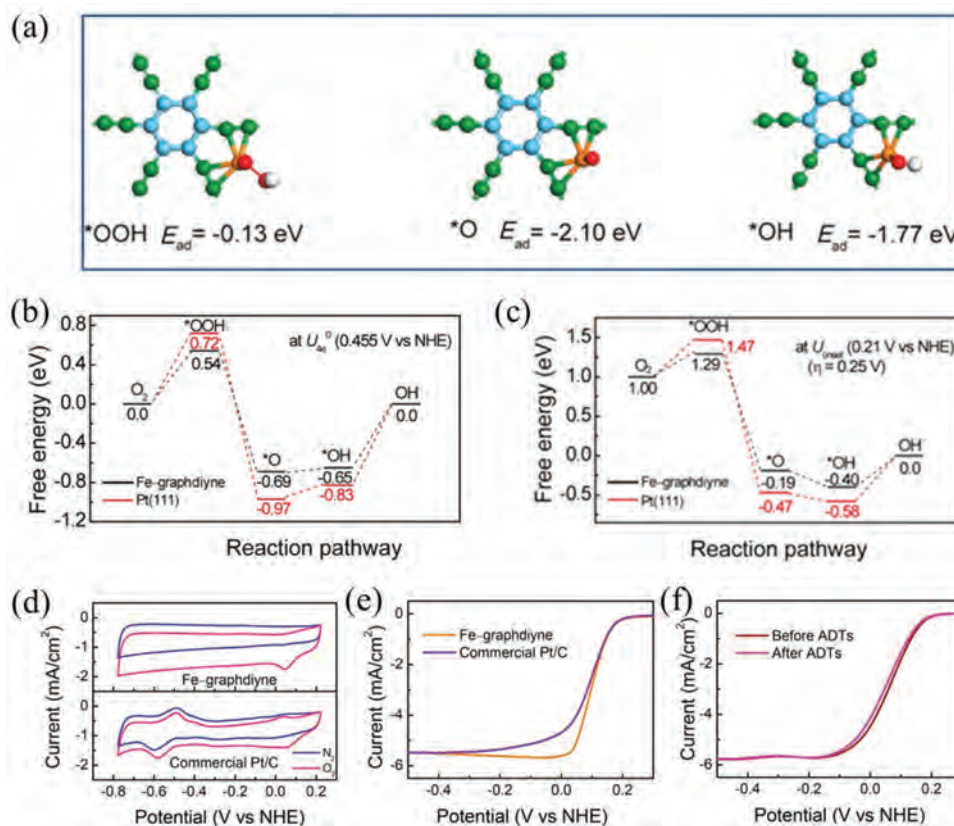


Figure 8. a) Top side views of the atomic configurations of *OOH, *O, and *OH adsorbed on Fe-graphdiyne surface. Atomic color code: pale blue, carbon in the C6 ring with sp² hybridization; green, carbon in the acetylenic-like rods with sp hybridization; orange, Fe; red, oxygen; and white, hydrogen atom. b,c) Calculated free energy diagrams of 4e⁻ pathways of the ORR at the Fe-graphdiyne and Pt (111) catalyst surfaces at the equilibrium electrode potential U_{eq}^0 (=0.455 V vs NHE, with $\eta = 0$ V) and at the experimental measured onset potential U_{onset} (=0.21 V vs NHE, with $\eta = 0.25$ V); d) Cyclic voltammetry (CV) responses of the Fe-graphdiyne catalyst (upper panel) and the commercial Pt/C catalyst (lower panel) in N₂-saturated (blue line) and O₂-saturated (red line) 0.1 M KOH solution at ambient temperature; e) Rotating disk electrode measurements in O₂-saturated 0.1 M KOH solution for Fe-graphdiyne catalyst (orange), and commercial 20 wt% Pt/C catalyst (violet); f) the stability of the Fe-graphdiyne catalyst for ORR. Reproduced with permission.^[134] Copyright 2018, American Chemical Society.

(111) catalyst (Figure 8b,c). In addition, the experiment results showed that the cathode peak potential of Fe-GDY for O₂ reduction was 53 mV, which was comparable to that of 20 wt% Pt/C catalyst (Figure 8d). However, Fe-GDY held much higher peak current of approximate 0.42 mA cm⁻², which was 1.68 times higher than that of 20 wt% Pt/C catalyst. Meanwhile, Fe-GDY possessed an identical Tafel slope with 20 wt% Pt/C, all above-mentioned results discovered that Fe-GDY electrocatalyst possessed predominant electrocatalytic performance for ORR. In addition, Fe-GDY electrocatalyst also owned the onset potential of 0.21 V, half-wave potential of 0.10 V, kinetic current density of 6.70 mA cm⁻², and rate constant of 1.47×10^{-5} (Figure 8e), which were equal to or even slightly higher than that of 20 wt% Pt/C catalyst. All of these indicated that the kinetics for ORR on Fe-GDY hybrid material was relatively high. Meanwhile, another essential factor (stability) for ORR was also investigated, the result showed that there was vaguely negative shift of half-wave potential (11 mV) and trifling reduction of kinetic current density (8%) after accelerating durability tests (ADTs), confirming its ultrahigh stability (Figure 8f).

Furthermore, Lin's group also pointed out that GDY-supported Pt nanoparticles was a superior electrocatalyst for ORR based on DFT calculations.^[98] The results displayed that the adsorption energy between GDY and Pt nanoparticles was 8.93 eV, which was 2.13 times larger than the adsorption energy between graphene and Pt nanoparticles (4.19 eV), revealing that anchoring Pt nanoparticles on GDY surface was more stable than that anchoring it on graphene. And the adsorptions of O₂ molecule on Pt/GDY and Pt/graphene systems were also explored, the result revealed that O–O bond length in Pt/GDY system (0.1299–0.1367 nm) was almost equal to that in Pt/graphene (0.1291–0.1354 nm). In addition, the electrons migrated from Pt nanoparticles to O₂ were in the range of 0.27–0.44 e in Pt/GDY system, which were also comparable to that in Pt/graphene system. In terms of aforementioned results, Pt/GDY electrocatalyst possessed great electrocatalytic ability for ORR in promising fuel cell technology. In consideration of the superior optical and electrical features of GDY, more GDY-based materials will be developed for ORR.^[62,135]

3.2.4. Overall Water Splitting

Electrochemical water splitting is regarded as a clean and sustainable route to generate hydrogen and oxygen for energy conversion.^[136] Therein, OER plays the critical role in OWS since the energy conversion efficiency of OWS is commonly limited by four consecutive proton-and-electron-transfer processes of OER, which generally results in sluggish kinetics and requires high overpotential to accelerate OER process. Therefore, exploiting bifunctional electrocatalyst for both OER and HER is of significance for driving OWS at low overpotential.^[137] As discussed in Section 3.2.2, GDY-based catalysts showed excellent performance for OER, which were equivalent with state-of-the-art Pt/C electrocatalyst. Thus, GDY-based materials also showed great potential for OWS.

In 2017, Li and his co-workers first used 3D GDY as support and NiCo₂S₄ as building blocks to synthesize a novel electrocatalyst.^[138] This electrocatalyst not only exhibited

high electrocatalytic performance for HER and OER, but also displayed remarkable electrocatalytic performance for OWS. As far as we know, NiCo₂S₄/GDY was the first GDY-based electrocatalyst that employed for OWS. As for OER and HER, NiCo₂S₄/GDY only needed the overpotentials of 308 and 170 mV to achieve the current density of 20 mA cm⁻¹. When NiCo₂S₄/GDY was used as both anode and cathode material for OWS, it also exhibited prominent catalytic performance with the cell voltages of 1.53, 1.56, 1.61, and 1.67 V to reach current densities of 10, 20, 50, and 100 mA cm⁻², respectively, which was much lower than that of NiCo₂S₄ NW/CC||NiCo₂S₄ NW/CC, GDY||GDY, CC||CC, and RuO₂||Pt/C. In addition, the catalytic performance of NiCo₂S₄/GDY was better than that of graphene and other carbon-material-based electrocatalysts which reported by previous studies (before 2017).^[139] From this example, GDY-based electrocatalysts show great potential for OWS and more and more GDY-based materials are expected to be developed for OWS.

Very recently, Li and co-workers prepared a bifunctional catalyst of GDY-wrapped cobalt nitride nanosheets on Ni foam (CoN_x@GDY NS/NF) through in situ growth method and employed it for OWS for the first time.^[91] The DFT result suggested that CoN_x@GDY had a relatively small H₂O activation energy (ΔG_1 , 0.45 eV), which was much smaller than that of benchmarked electrocatalysts such as Ni₂P (1.16 eV) and NiMoP (0.84 eV) (Figure 9a,c).^[140] It also possessed a small H adsorption energy of 0.05 eV, which was similar with Pt catalyst. All of these results suggested that CoN_x@GDY catalyzed HER proceeded an energy-favorable Volmer–Heyrovsky pathway, further revealing its high catalytic activity. In addition, the adsorption model of OER path revealed that the barrier from *OH to *OOH during OER process in CoN_x@GDY system was 3.27 eV, which was in line with previously reported studies.^[141] Meanwhile, the energy barrier of rate-determining step (generating *OOH) in CoN_x@GDY system was 2.75 eV, these results disclosed its essential active feature (Figure 9b,d). The electrochemical performance test showed that CoN_x@GDY NS/NF merely demanded the low overpotentials of 70 and 260 mV for HER and OER to obtain the catalytic current density of 10 mA cm⁻², which were superior to that of CoN_x NS/NF, Co-LDH NS/NF, pristine GDY, NF, and even Pt/C (Figure 9e,f). In addition, CoN_x@GDY NS/NF also possessed the smallest Tafel slope of 83 and 84 mV decade⁻¹ among CoN_x NS/NF (122 and 104 mV decade⁻¹), Co-LDH NS/NF (103 mV and 94 decade⁻¹), GDY (175 and 103 mV decade⁻¹) and NF (120 mV and 233 decade⁻¹) for HER and OER (Figure 9g,h), which confirmed its fast kinetics. More importantly, CoN_x@GDY NS/NF exhibited long-term durability since no palpable attenuation of electrocatalytic performance can be observed before and after several thousand operations under the same condition (Figure 9i,j). Considering the high catalytic performance of CoN_x@GDY NS/NF for HER and OER, CoN_x@GDY NS/NF can be straightforwardly used as electrode materials for OWS at alkaline medium. The results displayed that CoN_x@GDY NS/NF only needed relatively low cell voltage of 1.48 V to achieve the current density of 10 mA cm⁻², which was lower than that of other prepared materials and comparable to or even slightly superior to that of recently developed catalysts (Table 2).^[142–156] Furthermore, this CoN_x@GDY NS/NF also stayed almost high

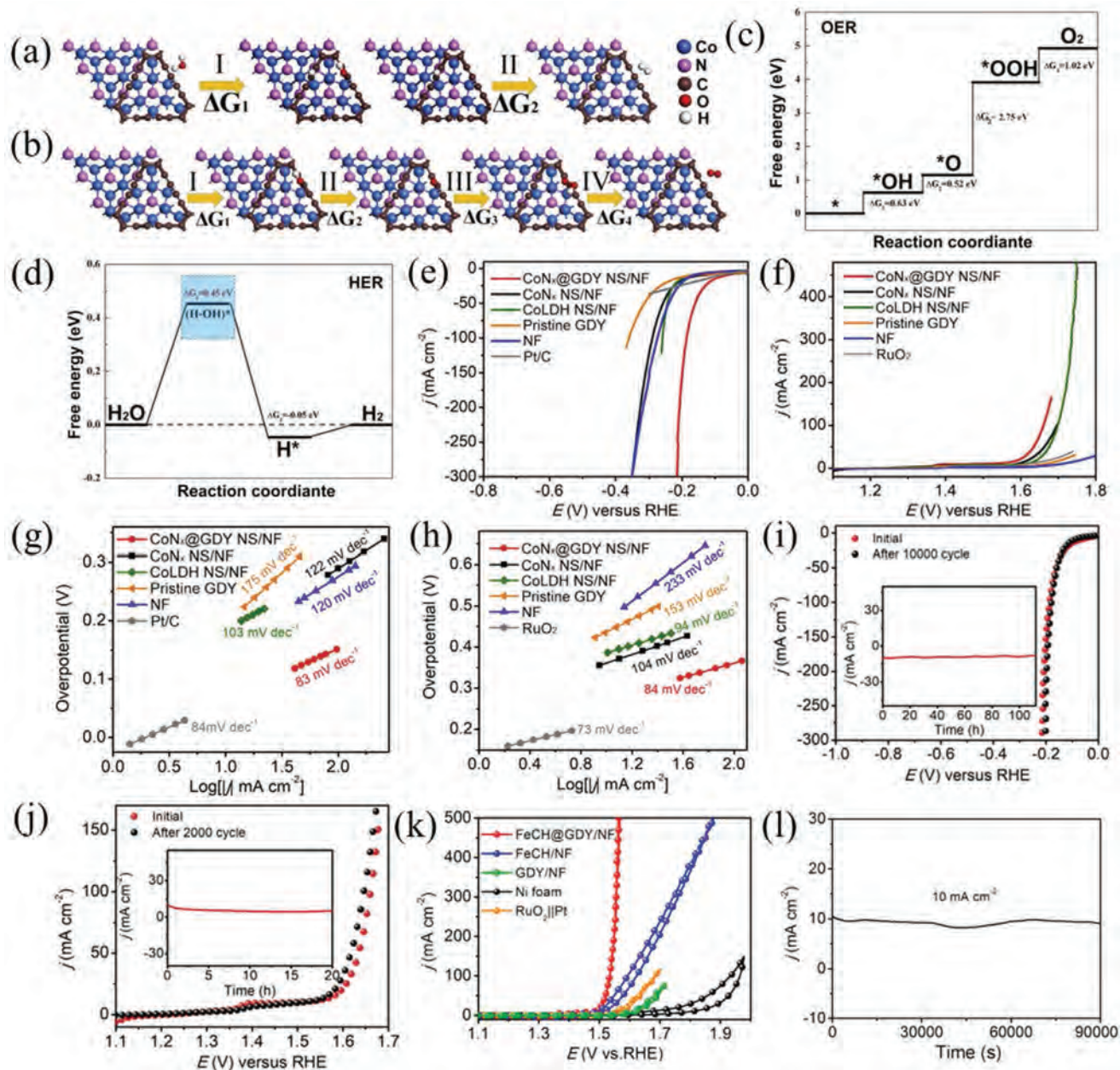


Figure 9. Chemisorption models for the calculated free energies toward a) HER and b) OER processes; c) calculated free energy diagram for H₂O activation and H adsorption in alkaline condition; d) free energy diagram for OER in alkaline media; e–f) polarization curves; g, h) corresponding Tafel plots of as-synthesized samples for HER and OER in 1.0 M KOH; i) polarization curves of CoN_x@GDY NS/NF before and after 10 000 cycles (inset: time-dependent current density curve of CoN_x@GDY NS/NF at an overpotential of –72 mV vs RHE for 110 h); j) polarization curves of CoN_x@GDY NS/NF before and after 2000 cycles (inset: time-dependent current density curve of CoN_x@GDY NS/NF at an overpotential of 280 mV versus RHE for 20 h). Reproduced with permission.^[91] Copyright 2019, Elsevier B.V. k) CV curves for as-synthesized samples in a two-electrode system; l) time-dependent current density curves of FeCH@GDY/NF at 10 mA cm⁻² in an alkaline electrolyzer. Reproduced with permission.^[87] Copyright 2018, American Chemical Society.

current density of 10 mA cm⁻² within 20 hours, further corroborating its strong durability.

Moreover, Li and his co-workers also prepared another bi-functional catalyst of GDY-wrapped iron carbonate hydroxide nanosheet (FeCH@GDY).^[87] The prepared FeCH@GDY nanomaterial exhibited predominant HER and OER performance with small overpotentials of 148 and 260 mV at 10 mA cm⁻². In

addition, when employing FeCH@GDY/NF as electrode materials for OWS, it demanded cell voltages of 1.49 and 1.53 V to realize the currents of 10 and 100 mA cm⁻² (Figure 9k). These were extremely low values among state-of-the-art electrocatalysts (Table 2), promulgating high performance of FeCH@GDY for OWS. More notably, long-term stability was detected in the FeCH@GDY||FeCH@GDY electrolyzer since no obvious

Table 2. The overall water splitting of FeCH@GDY/NF compared to state-of-the-art catalysts.

Catalysts	Electrolyte	Current density [mA cm^{-2}]	OER overpotentials [mV]	HER overpotentials [mV]	$E_{j=10}$ [V]	Times [h]
$\text{Ni}_3\text{FeN/r-GO}$ ^[142]	1.0 M KOH	10	270	94	1.60	100
$\text{Co}_{0.9}\text{S}_{0.58}\text{P}_{0.42}$ ^[143]	0.5 M H_2SO_4	10	266	139	1.59	30
CoSn_2 ^[144]	1.0 M KOH	10	299	196	1.55	16
$\text{PdP}_2\text{@CB}$ ^[145]	1.0 M KOH	50	270	46.6	1.72	10
Co-P/NC ^[146]	1.0 M KOH	165	319	−154	2.00	24
CF@FeCoS/NC ^[147]	1.0 M KOH	10	228	89	1.60	24
$\text{Ir}_6\text{Ag}_9\text{ NTs/C}$ ^[148]	0.5 M H_2SO_4	10	285	20	1.55	6
EBP@NC ^[149]	1.0 M KOH	10	310	125	1.54	12
CoFe@NiFe/NF ^[150]	1.0 M KOH	10	190	240	1.59	24
$\text{Co(OH)}_2\text{@NCNTs@NF}$ ^[151]	1.0 M KOH	10	270	170	1.72	600
$\text{Ni}_3\text{N-VN/NF}$ and $\text{Ni}_2\text{P-VP}_2\text{/NF}$ ^[152]	1.0 M KOH	10	220	37	1.51	100
$\text{N-NiMoO}_4\text{/NiS}_2$ ^[153]	1.0 M KOH	10	283	99	1.60	20
Fe, Co-NiSe_2 ^[154]	1.0 M KOH	10	251	92	1.52	30
$\text{NF-Ni}_3\text{S}_2\text{/MnO}_2$ ^[155]	1.0 M KOH	10	260	102	1.52	48
$\text{EG/H-Co}_{0.85}\text{Se P}$ ^[156]	0.01 M Na_2SO_4	10	–	150	1.64	2
$\text{CoN}_x\text{@GDY}$ ^[91]	1 M KOH	10	260	70	1.4	20
FeCH@GDY/NF ^[87]	1 M KOH	10	260	148	1.49	–

overpotential reduction can be observed after 90 000 cycles (Figure 9l). Meanwhile, SEM measurement revealed that the morphology did not change after successive operations, further indicating the robust structure of FeCH@GDY/NF. In a word, the emergence of 2D single-layer GDY offered innovative tactic to design and prepare low-price, high-performance, and strongly stable catalysts for HER, OER, and OWS, thereby providing clean and sustainable energy for future.

3.2.5. Nitrogen Reduction Reaction

Ammonia (NH_3) has been widely believed as the synthetic building blocks of manufacturing synthetic chemicals.^[157] In addition, NH_3 is also considered as a promising energy carrier in today's low-carbon society because of its high hydrogen content (17.6 wt%) and gravimetric energy density (4.3 kW h kg^{-1}).^[158] The ever-increasing NH_3 requirement has provoked great enthusiasm for artificial N_2 fixation.^[159] Up to present, the NH_3 synthesis is primarily dependent on Haber-Bosch process, while the huge energy input, low throughput, large greenhouse gas emission, and serious preparation prerequisite increase its operating costs.^[160] Electrochemical NRR from N_2 and H_2O with facile requirement is a potential channel, which could achieve sustainable and high yield of NH_3 .

In 2019, Huang's group first fabricated GDY-supported zerovalent molybdenum atoms catalyst ($\text{Mo}^0\text{/GDY}$) and applied it to NRR under acidic and alkaline conditions.^[115] The bonding and antibonding orbitals around Fermi level demonstrated that zerovalent Mo atoms were active sites. The Mo atoms migrated charge and amended charge allocation from C sites, thereby acting as electronic-rich cores to accelerate electron migration. Besides, NRR result showed that the Faradaic efficiencies

(FEs) of $\text{Mo}^0\text{/GDY}$ electrocatalyst varied in the range of $114\text{--}146 \mu\text{g h}^{-1} \text{mg}_{\text{cat}}^{-1}$ and NH_3 yield rates (Y_r) changed from 15.2% to 21.0% (Figure 10a–d), which were comparable to that of newly developed catalysts.^[161] Moreover, no NH_3 was observed in Ar-saturated 0.1 M HCl electrolyte and GDY displayed slight performance for NRR (Figure 10e,f), confirming that the generation of NH_3 was originated from N_2 reduction by $\text{Mo}^0\text{/GDY}$. In addition, other nitrogen compounds (for example, N_2H_4) could not be detected in this system, revealing the high selectivity of this hybrid material. Various characterizations showed that Mo atoms on GDY were stable and well-preserved during electrocatalytic measurement, which suggested the ultrahigh stability of this $\text{Mo}^0\text{/GDY}$ composite. Besides, the NRR measurement was also carried out at acid environment (0.1 M HCl electrolyte). Compared to pristine GDY, $\text{Mo}^0\text{/GDY}$ showed superior electrocatalytic performance with Y_r of $2.0 \mu\text{g}_{\text{NH}_3}\text{h}^{-1} \text{mg}_{\text{cat}}^{-1}$ and FEs of 15.6% at -0.1 V (Figure 10g–i). The above-stated evidences discovered that GDY-supported materials exhibited huge foreground for NRR.

4. Conclusion and Prospect

GDY, a novel 2D carbon material with sp^2 - and sp^3 -cohybridized carbon atoms, is a new member of carbon allotropes. After successful preparation, GDY has attracted tremendous interest owing to its laminated structure, high degree π -conjugation, regular ordered pore structure, and tunable electronic structure. In addition, the natural bandgap and Dirac cones structure of GDY also arouse huge attentions and many researchers have devoted efforts to investigating its physical and chemical properties and various applications. In this work, we have summarized the structures and properties

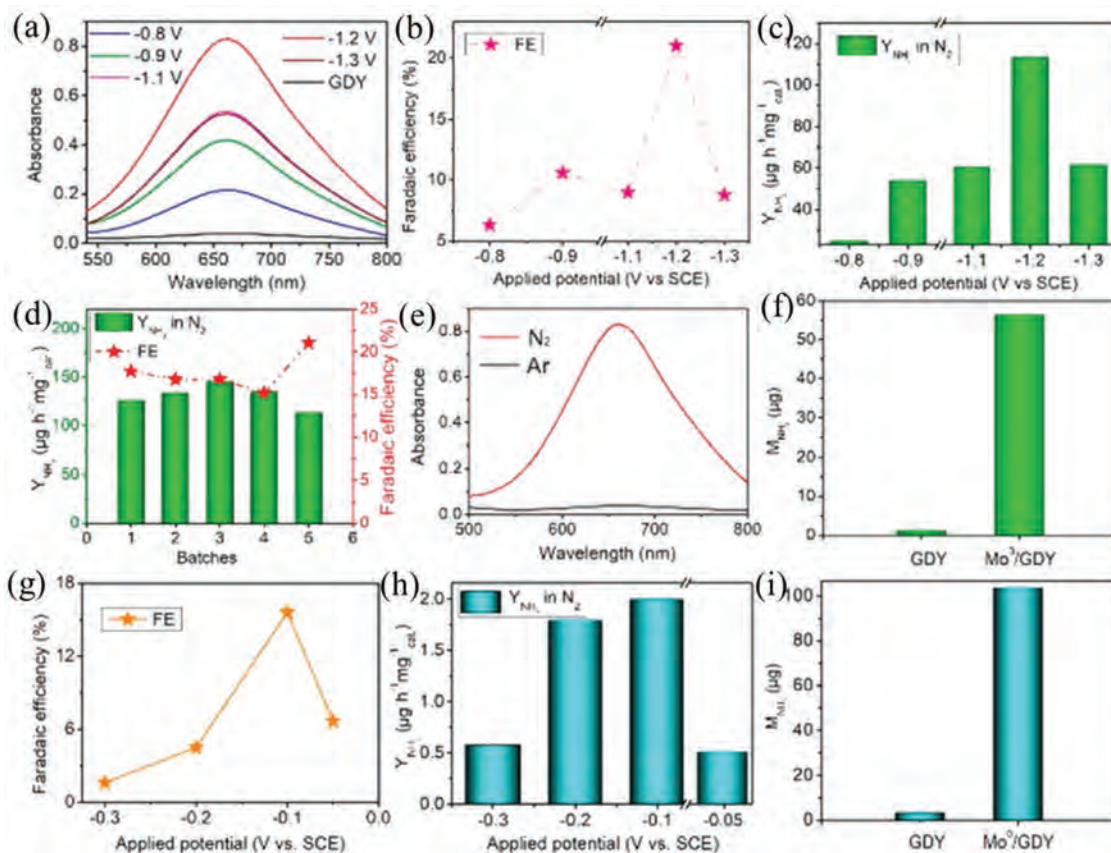


Figure 10. Electrochemical NRR performance of Mo⁰/GDY electrocatalyst. a) UV-vis absorption spectra of the 0.1 M Na₂SO₄ electrolytes after electrochemical NRR at different potentials for 2 h; b) FEs and c) Y_{NH₃} at different applied potentials in 0.1 M Na₂SO₄; d) Y_{NH₃} and FEs of NH₃ production of different batches of Mo⁰/GDY electrocatalyst; e) UV-vis adsorption spectra of Mo⁰/GDY electrocatalyst tested under N₂ (red line)-saturated and Ar (black line)-saturated electrolytes; f) amounts of NH₃ generated with pure GDY and the Mo⁰/GDY electrocatalyst after 2 h of electrolysis at -1.2 V under ambient conditions; g) FEs and h) Y_{NH₃} at different applied potentials in 0.1 M HCl; i) amounts of NH₃ generated with pure GDY and the Mo⁰/GDY electrocatalyst after 2 h of electrolysis at -0.1 V under ambient conditions. Reproduced with permission.^[115] Copyright 2019, American Chemical Society.

of GDY, which include molecular structure, electronic properties, mechanical properties, and stability. Based on these properties, we have discussed the feasibility of GDY as a support for electrocatalysts. Then, various GDY-supported electrocatalysts are reviewed and the roles of GDY in these hybrid materials are highlighted. Concretely, the presence of GDY can enhance the transfer efficiency of charge carrier, improve the dispersion, increase the electrical conductivity, and accelerate the mass transport. Finally, the electrochemical applications of GDY-supported electrocatalysts for energy conversion are first reviewed, and results reveal that GDY-supported electrocatalysts possess high performance for various electrochemical applications, including HER, OER, ORR, OWS, and NRR.

Although some achievements have been made for GDY-based electrocatalysts in energy conversion, researches in this field are still at their primary stage and many challenges and chances still exist. First of all, it is urgent to develop techniques for synthesizing large-scale, high-level, and affordable GDY and GYs, thereby providing stable foundation for theoretical studies and practical applications. Secondly, except for GDY, the fabrication methods of other GYs with different acetylene linkages such as GY, GY-3, and GY-4 are still in

the theoretical stage. Therefore, it is worth looking forward to obtaining GY, GY-3, and GY-4 with tunable structures and properties from laboratory. Thirdly, more state-of-the-art characterization techniques should be employed to thoroughly understand the connection among structure, property, and performance from molecular level and even atomic level. Fourthly, other modifications such as doping and surface functionalization should be explored to modify GDY with desired band gap, electronic properties, mechanical properties, and optical properties. Finally, the application scopes of GDY should not be limited to energy conversion. Because GDY also exhibits great potentials in other applications such as sensor, drug carrier, gas separation, battery, supercapacitor, and seawater desalination, but current researches in these aspects are in their infancy and lots of efforts are still needed to devote. In other words, more efforts should be invested to exploit GDY-based material for practical application. We believe that all challenges and shortcomings can be conquered and GDY-based material will be applied to various practical applications. We hope that this work could offer in-depth understanding of GDY for readers and give an available guidance for the fabrication and application of GDY-based materials in related domains.

Acknowledgements

This study was financially supported by the Program for the National Natural Science Foundation of China (51779090, 51879101, 51579098, 51709101, 51521006, 51809090, and 51909084), the National Program for Support of Top-Notch Young Professionals of China (2014), the Program for Changjiang Scholars and Innovative Research Team in University (IRT-13R17), Hunan Provincial Science and Technology Plan Project (2018SK20410, 2017SK2243, and 2016RS3026), and the Fundamental Research Funds for the Central Universities (531119200086, 531118010114, 531107050978, and 541109060031).

Conflict of Interest

The authors declare no conflict of interest.

Keywords

electrocatalysis, energy conversion, graphdiyne

Received: January 16, 2020

Revised: February 19, 2020

Published online:

- [1] a) T. S. Zeleke, M. C. Tsai, M. A. Weret, C. J. Huang, M. K. Birhanu, T. C. Liu, C. P. Huang, Y. L. Soo, Y. W. Yang, W. N. Su, B. J. Hwang, *ACS Nano* **2019**, *13*, 6720; b) B. Seo, G. Y. Jung, S. J. Lee, D. S. Baek, Y. J. Sa, H. W. Ban, J. S. Son, K. Park, S. K. Kwak, S. H. Joo, *ACS Catal.* **2020**, *10*, 652; c) M. D. Hossain, Z. Liu, M. Zhuang, X. Yan, G. L. Xu, C. A. Gadre, A. Tyagi, I. H. Abidi, C. J. Sun, H. Wong, A. Guda, Y. Hao, X. Pan, K. Amine, Z. Luo, *Adv. Energy Mater.* **2019**, *9*, 1803689.
- [2] S. Chu, Y. Cui, N. Liu, *Nat. Mater.* **2017**, *16*, 16.
- [3] a) C. A. Aubin, S. Choudhury, R. Jerch, L. A. Archer, J. H. Pikul, R. F. Shepherd, *Nature* **2019**, *571*, 51; b) X. Li, Y. Sun, J. Xu, Y. Shao, J. Wu, X. Xu, Y. Pan, H. Ju, J. Zhu, Y. Xie, *Nat. Energy* **2019**, *4*, 690; c) P. Boldrin, N. P. Brandon, *Nat. Catal.* **2019**, *2*, 571; d) C. Duan, R. Kee, H. Zhu, N. Sullivan, L. Zhu, L. Bian, D. Jennings, R. O'Hayre, *Nat. Energy* **2019**, *4*, 230; e) X. Wu, X. Ji, *Nat. Chem.* **2019**, *11*, 680; f) H. Xiong, L. Wu, Y. Liu, T. Gao, K. Li, Y. Long, R. Zhang, L. Zhang, Z. A. Qiao, Q. Huo, X. Ge, S. Song, H. Zhang, *Adv. Energy Mater.* **2019**, *9*, 1901634; g) K. S. Lee, S. Maurya, Y. S. Kim, C. R. Kreller, M. S. Wilson, D. Larsen, S. E. Elangovan, R. Mukundan, *Energy Environ. Sci.* **2018**, *11*, 979; h) Z. Liu, A. Zhou, J. Zhang, S. Wang, Y. Luan, W. Liu, A. Wang, X. Yue, *ACS Sustainable Chem. Eng.* **2018**, *6*, 3870; i) K. Verbeeck, L. C. Buelens, V. V. Galvita, G. B. Marin, K. M. Van Geem, K. Rabaey, *Energy Environ. Sci.* **2018**, *11*, 1788.
- [4] Y. Li, M. B. Majewski, S. M. Islam, S. Hao, A. A. Murthy, J. G. DiStefano, E. D. Hanson, Y. Xu, C. Wolverton, M. G. Kanatzidis, M. R. Wasielewski, X. Chen, V. P. Dravid, *Nano Lett.* **2018**, *18*, 7104.
- [5] C. H. Chen, D. Wu, Z. Li, R. Zhang, C. G. Kuai, X. R. Zhao, C. K. Dong, S. Z. Qiao, H. Liu, X. W. Du, *Adv. Energy Mater.* **2019**, *9*, 1803913.
- [6] K. Y. Kim, J. Lee, S. Kang, Y. W. Son, H. W. Jang, Y. Kang, S. Han, *ACS Catal.* **2018**, *8*, 4508.
- [7] L. Yu, H. Zhou, J. Sun, F. Qin, F. Yu, J. Bao, Y. Yu, S. Chen, Z. Ren, *Energy Environ. Sci.* **2017**, *10*, 1820.
- [8] H. Zhang, S. Hwang, M. Wang, Z. Feng, S. Karakalos, L. Luo, Z. Qiao, X. Xie, C. Wang, D. Su, Y. Shao, G. Wu, *J. Am. Chem. Soc.* **2017**, *139*, 14143.
- [9] J. Liu, Q. Ma, Z. Huang, G. Liu, H. Zhang, *Adv. Mater.* **2019**, *31*, 1800696.
- [10] I. Y. Kim, S. Kim, X. Jin, S. Premkumar, G. Chandra, N. S. Lee, G. P. Mane, S. J. Hwang, S. Umapathy, A. Vinu, *Angew. Chem., Int. Ed.* **2018**, *57*, 17135.
- [11] Y. Zhao, J. Zhang, W. Wu, X. Guo, P. Xiong, H. Liu, G. Wang, *Nano Energy* **2018**, *54*, 129.
- [12] W. Zhang, X. Zhang, L. Chen, J. Dai, Y. Ding, L. Ji, J. Zhao, M. Yan, F. Yang, C. R. Chang, S. Guo, *ACS Catal.* **2018**, *8*, 8092.
- [13] A. Safakas, G. Bamos, S. Bebelis, *Appl. Catal., B* **2019**, *244*, 225.
- [14] H. Bao, L. Wang, C. Li, J. Luo, *ACS Appl. Mater. Interfaces* **2019**, *11*, 2717.
- [15] R. H. Baughman, H. Eckhardt, M. Kertesz, *J. Chem. Phys.* **1987**, *87*, 6687.
- [16] C. Ge, J. Chen, S. Tang, Y. Du, N. Tang, *ACS Appl. Mater. Interfaces* **2019**, *11*, 2707.
- [17] C. Huang, Y. Li, N. Wang, Y. Xue, Z. Zuo, H. Liu, Y. Li, *Chem. Rev.* **2018**, *118*, 7744.
- [18] D. Malko, C. Neiss, A. Görling, *Phys. Rev. B* **2012**, *86*, 6335.
- [19] a) M. S. Hybertsen, S. G. Louie, *Phys. Rev. B* **1986**, *34*, 5390; b) J. Chen, J. Xi, D. Wang, Z. Shuai, *J. Phys. Chem. Lett.* **2013**, *4*, 1443.
- [20] S. W. Cranford, M. J. Buehler, *Carbon* **2011**, *49*, 4111.
- [21] Y. Y. Zhang, Q. X. Pei, C. M. Wang, *Appl. Phys. Lett.* **2012**, *101*, 666.
- [22] G. Li, Y. Li, H. Liu, Y. Guo, Y. Li, D. Zhu, *Chem. Commun.* **2010**, *46*, 3256.
- [23] H. Shang, Z. Zuo, L. Yu, F. Wang, F. He, Y. Li, *Adv. Mater.* **2018**, *30*, 1801459.
- [24] a) J. He, N. Wang, Z. Cui, H. Du, L. Fu, C. Huang, Z. Yang, X. Shen, Y. Yi, Z. Tu, Y. Li, *Nat. Commun.* **2017**, *8*, 1172; b) H. Du, Z. Zhang, J. He, Z. Cui, J. Chai, J. Ma, Z. Yang, C. Huang, G. Cui, *Small* **2017**, *13*, 1702277; c) N. Wang, J. He, K. Wang, Y. Zhao, T. Jiu, C. Huang, Y. Li, *Adv. Mater.* **2019**, *31*, 1803202.
- [25] a) J. Li, X. Gao, B. Liu, Q. Feng, X. B. Li, M. Y. Huang, Z. Liu, J. Zhang, C. H. Tung, L. Z. Wu, *J. Am. Chem. Soc.* **2016**, *138*, 3954; b) J. Li, Z. Xie, Y. Xiong, Z. Li, Q. Huang, S. Zhang, J. Zhou, R. Liu, X. Gao, C. Chen, L. Tong, J. Zhang, Z. Liu, *Adv. Mater.* **2017**, *29*, 1700421; c) X. Gao, J. Li, R. Du, J. Zhou, M. Y. Huang, R. Liu, J. Li, Z. Xie, L. Z. Wu, Z. Liu, J. Zhang, *Adv. Mater.* **2017**, *29*, 1605308; d) Z. Zuo, D. Wang, J. Zhang, F. Lu, Y. Li, *Adv. Mater.* **2019**, *31*, 1803762; e) J. Li, X. Gao, L. Zhu, M. N. Ghazzal, J. Zhang, C. H. Tung, L. Z. Wu, *Energy Environ. Sci.* **2020**, <https://doi.org/10.1039/C9EE03558C>.
- [26] a) J. Li, T. Jiu, S. Chen, L. Liu, Q. Yao, F. Bi, C. Zhao, Z. Wang, M. Zhao, G. Zhang, Y. Xue, F. Lu, Y. Li, *Nano Lett.* **2018**, *18*, 6941; b) H. Li, R. Zhang, Y. Li, Y. Li, H. Liu, J. Shi, H. Zhang, H. Wu, Y. Luo, D. Li, Y. Li, Q. Meng, *Adv. Energy Mater.* **2018**, *8*, 1802012; c) M. Li, Z. K. Wang, T. Kang, Y. Yang, X. Gao, C. S. Hsu, Y. Li, L. S. Liao, *Nano Energy* **2018**, *43*, 47.
- [27] a) S. Li, Y. Chen, H. Liu, Y. Wang, L. Liu, F. Lv, Y. Li, S. Wang, *Chem. Mater.* **2017**, *29*, 6087; b) N. Parvin, Q. Jin, Y. Wei, R. Yu, B. Zheng, L. Huang, Y. Zhang, L. Wang, H. Zhang, M. Gao, H. Zhao, W. Hu, Y. Li, D. Wang, *Adv. Mater.* **2017**, *29*, 1606755; c) J. Xie, N. Wang, X. Dong, C. Wang, Z. Du, L. Mei, Y. Yong, C. Huang, Y. Li, Z. Gu, Y. Zhao, *ACS Appl. Mater. Interfaces* **2019**, *11*, 2579.
- [28] a) M. Bartolomei, E. Carmona-Novillo, G. Giorgi, *Carbon* **2015**, *95*, 1076; b) L. Zhao, P. Sang, S. Guo, X. Liu, J. Li, H. Zhu, W. Guo, *Appl. Surf. Sci.* **2017**, *405*, 455; c) Y. Dang, W. Guo, L. Zhao, H. Zhu, *ACS Appl. Mater. Interfaces* **2017**, *9*, 30002.
- [29] a) X. Gao, J. Zhou, R. Du, Z. Xie, S. Deng, R. Liu, Z. Liu, J. Zhang, *Adv. Mater.* **2016**, *28*, 168; b) J. Kou, X. Zhou, H. Lu, F. Wu, J. Fan, *Nanoscale* **2014**, *6*, 1865; c) J. Li, Y. Chen, J. Gao, Z. Zuo, Y. Li, H. Liu, Y. Li, *ACS Appl. Mater. Interfaces* **2019**, *11*, 2591.
- [30] A. L. Ivanovskii, *Prog. Solid State Chem.* **2013**, *41*, 1.

- [31] M. Ozmaian, A. Fathizadeh, M. Jalalvand, M. R. Ejtehadi, S. M. Allaei, *Sci. Rep.* **2016**, 6, 21910.
- [32] S. W. Cranford, D. B. Brommer, M. J. Buehler, *Nanoscale* **2012**, 4, 7797.
- [33] H. Bu, M. Zhao, H. Zhang, X. Wang, Y. Xi, Z. Wang, *J. Phys. Chem. A* **2012**, 116, 3934.
- [34] a) S. Zhang, J. Wang, Z. Li, R. Zhao, L. Tong, Z. Liu, J. Zhang, Z. Liu, *J. Phys. Chem. C* **2016**, 120, 10605; b) J. Li, J. Xu, Z. Xie, X. Gao, J. Zhou, Y. Xiong, C. Chen, J. Zhang, Z. Liu, *Adv. Mater.* **2018**, 30, 1800548; c) N. Yang, Y. Liu, H. Wen, Z. Tang, H. Zhao, Y. Li, D. Wang, *ACS Nano* **2013**, 7, 1504.
- [35] C. Hu, H. Liu, Y. Liu, J.-F. Chen, Y. Li, L. Dai, *Nano Energy* **2019**, 63, 103874.
- [36] Q. Zheng, G. Luo, Q. Liu, R. Quhe, J. Zheng, K. Tang, Z. Gao, S. Nagase, J. Lu, *Nanoscale* **2012**, 4, 3990.
- [37] Y. Yang, X. Xu, *Comput. Mater. Sci.* **2012**, 61, 83.
- [38] N. Narita, S. Nagai, S. Suzuki, K. Nakao, *Phys. Rev. B* **1998**, 58, 11009.
- [39] H. Bai, Y. Zhu, W. Qiao, Y. Huang, *RSC Adv.* **2011**, 1, 768.
- [40] M. Mirnezhad, R. Ansari, H. Rouhi, M. Seifi, M. Faghihnasiri, *Solid State Commun.* **2012**, 152, 1885.
- [41] Q. Peng, W. Ji, S. De, *Phys. Chem. Chem. Phys.* **2012**, 14, 13385.
- [42] Y. Pei, *Phys. B* **2012**, 407, 4436.
- [43] Y. Xue, Y. Li, J. Zhang, Z. Liu, Y. Zhao, *Sci. China: Chem.* **2018**, 61, 765.
- [44] G. Luo, X. Qian, H. Liu, R. Qin, J. Zhou, L. Li, Z. Gao, E. Wang, W. N. Mei, J. Lu, Y. Li, S. Nagase, *Phys. Rev. B* **2011**, 84, 075439.
- [45] Y. Jiao, A. Du, M. Hankel, Z. Zhu, V. Rudolph, S. C. Smith, *Chem. Commun.* **2011**, 47, 11843.
- [46] H. J. Cui, X. L. Sheng, Q. B. Yan, Q. R. Zheng, G. Su, *Phys. Chem. Chem. Phys.* **2013**, 15, 8179.
- [47] L. D. Pan, L. Z. Zhang, B. Q. Song, S. X. Du, H. J. Gao, *Appl. Phys. Lett.* **2012**, 98, 666.
- [48] B. G. Shohany, M. R. Roknabadi, A. Kompany, *Phys. E* **2016**, 84, 146.
- [49] D. Malko, C. Neiss, F. Viñes, A. Görling, *Phys. Rev. Lett.* **2012**, 108, 086804.
- [50] M. Long, L. Tang, D. Wang, Y. Li, Z. Shuai, *ACS Nano* **2011**, 5, 2593.
- [51] C. Lee, X. Wei, J. W. Kysar, J. Hone, *Science* **2008**, 321, 385.
- [52] J. Hou, Z. Yin, Y. Zhang, T. Chang, *J. Appl. Mech.* **2015**, 82, 094501.
- [53] S. Ajori, R. Ansari, M. Mirnezhad, *Mater. Sci. Eng., A* **2013**, 561, 34.
- [54] Y. Li, L. Xu, H. Liu, Y. Li, *Chem. Soc. Rev.* **2014**, 43, 2572.
- [55] A. N. Enyashin, A. L. Ivanovskii, *Phys. Status Solidi B* **2011**, 248, 1879.
- [56] M. M. Haley, S. C. Brand, J. J. Pak, *Angew. Chem., Int. Ed. Engl.* **1997**, 36, 836.
- [57] a) S. Zhu, J. Li, X. Deng, C. He, E. Liu, F. He, C. Shi, N. Zhao, *Adv. Funct. Mater.* **2017**, 27, 1605017; b) S. S. Shin, S. J. Lee, S. I. Seok, *Adv. Funct. Mater.* **2019**, 29, 1900455; c) T. Nguyen, M. F. Montemor, *Adv. Sci.* **2019**, 6, 1801797; d) T. Butburee, Y. Bai, H. Wang, H. Chen, Z. Wang, G. Liu, J. Zou, P. Khemthong, G. Q. M. Lu, L. Wang, *Adv. Mater.* **2018**, 30, 1705666.
- [58] a) S. Wan, M. Ou, Q. Zhong, S. Zhang, F. Song, *Chem. Eng. J.* **2017**, 325, 690; b) J. Han, D. Kong, W. Lv, D. M. Tang, D. Han, C. Zhang, D. Liu, Z. Xiao, X. Zhang, J. Xiao, X. He, F. C. Hsia, C. Zhang, Y. Tao, D. Golberg, F. Kang, L. Zhi, Q. H. Yang, *Nat. Commun.* **2018**, 9, 402.
- [59] D. J. Miller, C. Proff, J. G. Wen, D. P. Abraham, J. Bareño, *Adv. Energy Mater.* **2013**, 3, 1098.
- [60] a) H. Tabassum, R. Zou, A. Mahmood, Z. Liang, Q. Wang, H. Zhang, S. Gao, C. Qu, W. Guo, S. Guo, *Adv. Mater.* **2018**, 30, 1705441; b) Q. Li, P. Xu, W. Gao, S. Ma, G. Zhang, R. Cao, J. Cho, H. L. Wang, G. Wu, *Adv. Mater.* **2014**, 26, 1378.
- [61] a) Z. Jia, Y. Li, Z. Zuo, H. Liu, C. Huang, Y. Li, *Acc. Chem. Res.* **2017**, 50, 2470; b) H. Yu, Y. Xue, Y. Li, *Adv. Mater.* **2019**, 31, 1803101; c) Y. Y. Han, X. L. Lu, S. F. Tang, X. P. Yin, Z. W. Wei, T. B. Lu, *Adv. Energy Mater.* **2018**, 8, 1702992; d) J. Xiao, J. Shi, H. Liu, Y. Xu, S. Lv, Y. Luo, D. Li, Q. Meng, Y. Li, *Adv. Energy Mater.* **2015**, 5, 1401943; e) Y. Zhao, N. Yang, H. Yao, D. Liu, L. Song, J. Zhu, S. Li, L. Gu, K. Lin, D. Wang, *J. Am. Chem. Soc.* **2019**, 141, 7240; f) S. Guo, P. Yu, W. Li, Y. Yi, F. Wu, L. Mao, *J. Am. Chem. Soc.* **2020**, 142, 2074; g) H. Zou, W. Rong, B. Long, Y. Ji, L. Duan, *ACS Catal.* **2019**, 9, 10649.
- [62] W. Si, Z. Yang, X. Wang, Q. Lv, F. Zhao, X. Li, J. He, Y. Long, J. Gao, C. Huang, *ChemSusChem* **2019**, 12, 173.
- [63] H. Yu, Y. Xue, L. Hui, F. He, C. Zhang, Y. Liu, Y. Fang, C. Xing, Y. Li, H. Liu, Y. Li, *Nano Energy* **2019**, 64, 103928.
- [64] a) C. C. McCrory, S. Jung, I. M. Ferrer, S. M. Chatman, J. C. Peters, T. F. Jaramillo, *J. Am. Chem. Soc.* **2015**, 137, 4347; b) Y. Gorlin, B. Lassalle-Kaiser, J. D. Benck, S. Gul, S. M. Webb, V. K. Yachandra, J. Yano, T. F. Jaramillo, *J. Am. Chem. Soc.* **2013**, 135, 8525; c) J. Greeley, T. F. Jaramillo, J. Bonde, I. Chorkendorff, J. K. Nørskov, *Nat. Mater.* **2006**, 5, 909; d) I. Roger, M. A. Shipman, M. D. Symes, *Nat. Rev. Chem.* **2017**, 1, 0003; e) J. Zhang, T. Wang, D. Pohl, B. Rellinghaus, R. Dong, S. Liu, X. Zhuang, X. Feng, *Angew. Chem., Int. Ed.* **2016**, 55, 6702.
- [65] a) C. Tang, R. Zhang, W. Lu, L. He, X. Jiang, A. M. Asiri, X. Sun, *Adv. Mater.* **2017**, 29, 1602441; b) I. K. Mishra, H. Zhou, J. Sun, F. Qin, K. Dahal, J. Bao, S. Chen, Z. Ren, *Energy Environ. Sci.* **2018**, 11, 2246; c) F. Yu, H. Zhou, Y. Huang, J. Sun, F. Qin, J. Bao, W. A. Goddard, S. Chen, Z. Ren, *Nat. Commun.* **2018**, 9, 2551.
- [66] a) X. Zang, W. Chen, X. Zou, J. N. Hohman, L. Yang, B. Li, M. Wei, C. Zhu, J. Liang, M. Sanghadasa, J. Gu, L. Lin, *Adv. Mater.* **2018**, 30, 1805188; b) W. Liu, B. Chen, X. Duan, K. H. Wu, W. Qi, X. Guo, B. Zhang, D. Su, *ACS Catal.* **2017**, 7, 5820; c) L. Najafi, S. Bellani, R. Oropesa-Núñez, M. Prato, B. Martín-García, R. Brescia, F. Bonaccorso, *ACS Nano* **2019**, 13, 3162.
- [67] a) C. Panda, P. W. Menezes, C. Walter, S. Yao, M. E. Miehl, V. Gutkin, K. Meyer, M. Driess, *Angew. Chem., Int. Ed.* **2017**, 56, 10506; b) N. Masurkar, N. K. Thangavel, L. M. R. Arava, *ACS Appl. Mater. Interfaces* **2018**, 10, 27771; c) Q. Lu, Y. Yu, Q. Ma, B. Chen, H. Zhang, *Adv. Mater.* **2016**, 28, 1917.
- [68] a) Y. Zang, S. Niu, Y. Wu, X. Zheng, J. Cai, J. Ye, Y. Xie, Y. Liu, J. Zhou, J. Zhu, X. Liu, G. Wang, Y. Qian, *Nat. Commun.* **2019**, 10, 1217; b) D. R. Cummins, U. Martinez, A. Sherehiy, R. Kappera, A. Martinez-Garcia, R. K. Schulze, J. Jasinski, J. Zhang, R. K. Gupta, J. Lou, M. Chhowalla, G. Sumanasekera, A. D. Mohite, M. K. Sunkara, G. Gupta, *Nat. Commun.* **2016**, 7, 11857; c) X. Li, T. Li, Y. Ma, Q. Wei, W. Qiu, H. Guo, X. Shi, P. Zhang, A. M. Asiri, L. Chen, B. Tang, X. Sun, *Adv. Energy Mater.* **2018**, 8, 1801357.
- [69] a) L. Yang, W. Zhou, J. Lu, D. Hou, Y. Ke, G. Li, Z. Tang, X. Kang, S. Chen, *Nano Energy* **2016**, 22, 490; b) L. Qin, Z. Zeng, G. Zeng, C. Lai, A. Duan, R. Xiao, D. Huang, Y. Fu, H. Yi, B. Li, X. Liu, S. Liu, M. Zhang, D. Jiang, *Appl. Catal., B* **2019**, 259, 118035.
- [70] H. Yu, Y. Xue, L. Hui, C. Zhang, Y. Li, Z. Zuo, Y. Zhao, Z. Li, Y. Li, *Adv. Mater.* **2018**, 30, 1707082.
- [71] S. Zhuo, Y. Shi, L. Liu, R. Li, L. Shi, D. H. Anjum, Y. Han, P. Wang, *Nat. Commun.* **2018**, 9, 3132.
- [72] a) B. Li, C. Lai, G. Zeng, L. Qin, H. Yi, D. Huang, C. Zhou, X. Liu, M. Cheng, P. Xu, C. Zhang, F. Huang, S. Liu, *ACS Appl. Mater. Interfaces* **2018**, 10, 18824; b) B. Li, C. Lai, L. Qin, C. Chu, M. Zhang, S. Liu, X. Liu, H. Yi, J. He, L. Li, M. Li, L. Chen, *J. Colloid Interface Sci.* **2020**, 560, 701; c) B. Li, C. Lai, P. Xu, G. Zeng, D. Huang, L. Qin, H. Yi, M. Cheng, L. Wang, F. Huang, S. Liu, M. Zhang, *J. Cleaner Prod.* **2019**, 225, 898.
- [73] Y. Yao, Z. Jin, Y. Chen, Z. Gao, J. Yan, H. Liu, J. Wang, Y. Li, S. Liu, *Carbon* **2018**, 129, 228.

- [74] a) S. Yu, J. Kim, K. R. Yoon, J. W. Jung, J. Oh, I. D. Kim, *ACS Appl. Mater. Interfaces* **2015**, 7, 28116; b) Y. Li, C. Guo, J. Li, W. Liao, Z. Li, J. Zhang, C. Chen, *Carbon* **2017**, 119, 201.
- [75] H. Yu, Y. Xue, L. Hui, C. Zhang, Y. Zhao, Z. Li, Y. Li, *Adv. Funct. Mater.* **2018**, 28, 1707564.
- [76] a) Z. W. Gao, J. Y. Liu, X. M. Chen, X. L. Zheng, J. Mao, H. Liu, T. Ma, L. Li, W. C. Wang, X. W. Du, *Adv. Mater.* **2019**, 31, 1804769; b) T. Tang, W. J. Jiang, S. Niu, N. Liu, H. Luo, Q. Zhang, W. Wen, Y. Y. Chen, L. B. Huang, F. Gao, J. S. Hu, *Adv. Funct. Mater.* **2018**, 28, 1704594; c) R. Zhang, M. Shao, J. Xu, F. Ning, L. Zhou, M. Wei, *Nano Energy* **2017**, 33, 21; d) Y. Wang, Y. Zhang, Z. Liu, C. Xie, S. Feng, D. Liu, M. Shao, S. Wang, *Angew. Chem., Int. Ed.* **2017**, 56, 5867; e) L. Lv, Z. Yang, K. Chen, C. Wang, Y. Xiong, *Adv. Energy Mater.* **2019**, 9, 1803358.
- [77] a) Z. Wang, S. Zeng, W. Liu, X. Wang, Q. Li, Z. Zhao, F. Geng, *ACS Appl. Mater. Interfaces* **2017**, 9, 1488; b) M. Gong, Y. Li, H. Wang, Y. Liang, J. Z. Wu, J. Zhou, J. Wang, T. Regier, F. Wei, H. Dai, *J. Am. Chem. Soc.* **2013**, 135, 8452; c) S. Yin, W. Tu, Y. Sheng, Y. Du, M. Kraft, A. Borgna, R. Xu, *Adv. Mater.* **2018**, 30, 1705106.
- [78] J. Ping, Y. Wang, Q. Lu, B. Chen, J. Chen, Y. Huang, Q. Ma, C. Tan, J. Yang, X. Cao, Z. Wang, J. Wu, Y. Ying, H. Zhang, *Adv. Mater.* **2016**, 28, 7640.
- [79] Y. Ni, L. Yao, Y. Wang, B. Liu, M. Cao, C. Hu, *Nanoscale* **2017**, 9, 11596.
- [80] F. S. Zhang, J. W. Wang, J. Luo, R. R. Liu, Z. M. Zhang, C. T. He, T. B. Lu, *Chem. Sci.* **2018**, 9, 1375.
- [81] H. Zhang, X. Li, A. Hähnel, V. Naumann, C. Lin, S. Azimi, S. L. Schweizer, A. W. Majnenburg, R. B. Wehrspohn, *Adv. Funct. Mater.* **2018**, 28, 1706847.
- [82] M. Yu, S. Zhou, Z. Wang, J. Zhao, J. Qiu, *Nano Energy* **2018**, 44, 181.
- [83] L. Hui, Y. Xue, B. Huang, H. Yu, C. Zhang, D. Zhang, D. Jia, Y. Zhao, Y. Li, H. Liu, Y. Li, *Nat. Commun.* **2018**, 9, 5309.
- [84] J. Li, X. Gao, Z. Li, J. H. Wang, L. Zhu, C. Yin, Y. Wang, X. B. Li, Z. Liu, J. Zhang, C. H. Tung, L. Z. Wu, *Adv. Funct. Mater.* **2019**, 29, 1808079.
- [85] H. Li, T. N. Tran, B. J. Lee, C. Zhang, J. D. Park, T. H. Kang, J. S. Yu, *ACS Appl. Mater. Interfaces* **2017**, 9, 20294.
- [86] G. Shi, C. Yu, Z. Fan, J. Li, M. Yuan, *ACS Appl. Mater. Interfaces* **2019**, 11, 2662.
- [87] L. Hui, D. Jia, H. Yu, Y. Xue, Y. Li, *ACS Appl. Mater. Interfaces* **2019**, 11, 2618.
- [88] P. Kuang, B. Zhu, Y. Li, H. Liu, J. Yu, K. Fan, *Nanoscale Horiz.* **2018**, 3, 317.
- [89] S. Joshi, Q. Wang, A. Puntambekar, V. Chakrapani, *ACS Energy Lett.* **2017**, 2, 1257.
- [90] T. Zhou, W. Lv, J. Li, G. Zhou, Y. Zhao, S. Fan, B. Liu, B. Li, F. Kang, Q. H. Yang, *Energy Environ. Sci.* **2017**, 10, 1694.
- [91] Y. Fang, Y. Xue, L. Hui, H. Yu, Y. Liu, C. Xing, F. Lu, F. He, H. Liu, Y. Li, *Nano Energy* **2019**, 59, 591.
- [92] B. Li, C. Lai, G. Zeng, D. Huang, L. Qin, M. Zhang, M. Cheng, X. Liu, H. Yi, C. Zhou, F. Huang, S. Liu, Y. Fu, *Small* **2019**, 15, 1804565.
- [93] M. Govindhan, B. Mao, A. Chen, *Nanoscale* **2016**, 8, 1485.
- [94] a) X. N. Li, Z. Yuan, S. G. He, *J. Am. Chem. Soc.* **2014**, 136, 3617; b) H. Fei, J. Dong, Y. Feng, C. S. Allen, C. Wan, B. Voloskiy, M. Li, Z. Zhao, Y. Wang, H. Sun, P. An, W. Chen, Z. Guo, C. Lee, D. Chen, I. Shakir, M. Liu, T. Hu, Y. Li, A. I. Kirkland, X. Duan, Y. Huang, *Nat. Catal.* **2018**, 1, 63.
- [95] B. Qiao, A. Wang, X. Yang, L. F. Allard, Z. Jiang, Y. Cui, J. Liu, J. Li, T. Zhang, *Nat. Chem.* **2011**, 3, 634.
- [96] W. L. Wang, E. J. Santos, B. Jiang, E. D. Cubuk, C. Ophus, A. Centeno, A. Pesquera, A. Zurutuza, J. Ciston, R. Westervelt, E. Kaxiras, *Nano Lett.* **2014**, 14, 450.
- [97] Y. Xue, J. Li, Z. Xue, Y. Li, H. Liu, D. Li, W. Yang, Y. Li, *ACS Appl. Mater. Interfaces* **2016**, 8, 31083.
- [98] Z. Z. Lin, *Carbon* **2015**, 86, 301.
- [99] J. He, S. Y. Ma, P. Zhou, C. X. Zhang, C. He, L. Z. Sun, *J. Phys. Chem. C* **2012**, 116, 26313.
- [100] a) B. Li, S. Liu, C. Lai, G. Zeng, M. Zhang, M. Zhou, D. Huang, L. Qin, X. Liu, Z. Li, N. An, F. Xu, H. Yi, Y. Zhang, L. Chen, *Appl. Catal., B* **2020**, 266, 118650; b) M. Zhang, C. Lai, B. Li, D. Huang, G. Zeng, P. Xu, L. Qin, S. Liu, X. Liu, H. Yi, M. Li, C. Chu, Z. Chen, *J. Catal.* **2019**, 369, 469; c) C. Lai, M. Zhang, B. Li, D. Huang, G. Zeng, L. Qin, X. Liu, H. Yi, M. Cheng, L. Li, Z. Chen, L. Chen, *Chem. Eng. J.* **2019**, 358, 891.
- [101] J. Li, X. Gao, X. Jiang, X. B. Li, Z. Liu, J. Zhang, C. H. Tung, L. Z. Wu, *ACS Catal.* **2017**, 7, 5209.
- [102] a) S. Dou, C. L. Dong, Z. Hu, Y. C. Huang, J. I. Chen, L. Tao, D. Yan, D. Chen, S. Shen, S. Chou, S. Wang, *Adv. Funct. Mater.* **2017**, 27, 1702546; b) S. Dou, L. Tao, J. Huo, S. Wang, L. Dai, *Energy Environ. Sci.* **2016**, 9, 1320.
- [103] P. Liu, Y. Zhao, R. Qin, S. Mo, G. Chen, L. Gu, D. M. Chevrier, P. Zhang, Q. Guo, D. Zang, B. Wu, G. Fu, N. Zheng, *Science* **2016**, 352, 797.
- [104] Z. Y. Li, Z. Yuan, X. N. Li, Y. X. Zhao, S. G. He, *J. Am. Chem. Soc.* **2014**, 136, 14307.
- [105] a) S. Chen, N. Zhang, C. W. Narváez Villarrubia, X. Huang, L. Xie, X. Wang, X. Kong, H. Xu, G. Wu, J. Zeng, H. L. Wang, *Nano Energy* **2019**, 66, 104164; b) J. Deng, H. Li, J. Xiao, Y. Tu, D. Deng, H. Yang, H. Tian, J. Li, P. Ren, X. Bao, *Energy Environ. Sci.* **2015**, 8, 1594; c) C. Dong, X. Zhang, J. Xu, R. Si, J. Sheng, J. Luo, S. Zhang, W. Dong, G. Li, W. Wang, F. Huang, *Small* **2020**, 16, 1905328; d) Z. Wang, S. M. Xu, Y. Xu, L. Tan, X. Wang, Y. Zhao, H. Duan, Y. F. Song, *Chem. Sci.* **2019**, 10, 378; e) J. Yan, L. Kong, Y. Ji, J. White, Y. Li, J. Zhang, P. An, S. Liu, S.-T. Lee, T. Ma, *Nat. Commun.* **2019**, 10, 2149; f) J. Zhang, Y. Zhao, C. Chen, Y. C. Huang, C. L. Dong, C. J. Chen, R. S. Liu, C. Wang, K. Yan, Y. Li, G. Wang, *J. Am. Chem. Soc.* **2019**, 141, 20118.
- [106] a) Q. Zuo, T. Liu, C. Chen, Y. Ji, X. Gong, Y. Mai, Y. Zhou, *Angew. Chem.* **2019**, 131, 10304; b) F. Li, G. F. Han, H. J. Noh, S. J. Kim, Y. Lu, H. Y. Jeong, Z. Fu, J. B. Baek, *Energy Environ. Sci.* **2018**, 11, 2263; c) Q. Zhao, J. Sun, S. Li, C. Huang, W. Yao, W. Chen, T. Zeng, Q. Wu, Q. Xu, *ACS Catal.* **2018**, 8, 11863; d) S. Cao, H. Li, T. Tong, H. C. Chen, A. Yu, J. Yu, H. M. Chen, *Adv. Funct. Mater.* **2018**, 28, 1802169; e) S. Qiu, Y. Shen, G. Wei, S. Yao, W. Xi, M. Shu, R. Si, M. Zhang, J. Zhu, C. An, *Appl. Catal., B* **2019**, 259, 118036; f) V. Ramalingam, P. Varadhan, H. C. Fu, H. Kim, D. Zhang, S. Chen, L. Song, D. Ma, Y. Wang, H. N. Alshareef, J. H. He, *Adv. Mater.* **2019**, 31, 1903841.
- [107] X. P. Yin, H. J. Wang, S. F. Tang, X. L. Lu, M. Shu, R. Si, T. B. Lu, *Angew. Chem., Int. Ed.* **2018**, 57, 9382.
- [108] N. Cheng, S. Stambula, D. Wang, M. N. Banis, J. Liu, A. Riese, B. Xiao, R. Li, T. K. Sham, L. M. Liu, G. A. Botton, X. Sun, *Nat. Commun.* **2016**, 7, 13638.
- [109] a) B. Hinnemann, P. G. Moses, J. Bonde, K. P. Jørgensen, J. H. Nielsen, S. Horch, I. Chorkendorff, J. K. Nørskov, *J. Am. Chem. Soc.* **2005**, 127, 5308; b) X. Li, W. Bi, L. Zhang, S. Tao, W. Chu, Q. Zhang, Y. Luo, C. Wu, Y. Xie, *Adv. Mater.* **2016**, 28, 2427.
- [110] Z. Z. Lin, *Carbon* **2016**, 108, 343.
- [111] T. He, S. K. Matta, G. Will, A. Du, *Small Methods* **2019**, 3, 1800419.
- [112] Y. Xue, B. Huang, Y. Yi, Y. Guo, Z. Zuo, Y. Li, Z. Jia, H. Liu, Y. Li, *Nat. Commun.* **2018**, 9, 1460.
- [113] H. Yu, Y. Xue, B. Huang, L. Hui, C. Zhang, Y. Fang, Y. Liu, Y. Zhao, Y. Li, H. Liu, Y. Li, *iScience* **2019**, 11, 31.
- [114] B. Huang, *Phys. Chem. Chem. Phys.* **2017**, 19, 8008.
- [115] L. Hui, Y. Xue, H. Yu, Y. Liu, Y. Fang, C. Xing, B. Huang, Y. Li, *J. Am. Chem. Soc.* **2019**, 141, 10677.

- [116] a) W. Xie, Y. Song, S. Li, J. Li, Y. Yang, W. Liu, M. Shao, M. Wei, *Adv. Funct. Mater.* **2019**, 29, 1906477; b) B. Yu, H. Li, J. White, S. Donne, J. Yi, S. Xi, Y. Fu, G. Henkelman, H. Yu, Z. Chen, T. Ma, *Adv. Funct. Mater.* **2020**, 30, 1905665; c) P. Huang, M. Cheng, H. Zhang, M. Zuo, C. Xiao, Y. Xie, *Nano Energy* **2019**, 61, 428; d) L. Wang, X. Duan, X. Liu, J. Gu, R. Si, Y. Qiu, Y. Qiu, D. Shi, F. Chen, X. Sun, J. Lin, J. Sun, *Adv. Energy Mater.* **2020**, 10, 1903137; e) G. Han, Y. Zheng, X. Zhang, Z. Wang, Y. Gong, C. Du, M. N. Banis, Y. M. Yiu, T. K. Sham, L. Gu, Y. Sun, Y. Wang, J. Wang, Y. Gao, G. Yin, X. Sun, *Nano Energy* **2019**, 66, 104088.
- [117] K. Li, Y. Li, Y. Wang, J. Ge, C. Liu, W. Xing, *Energy Environ. Sci.* **2018**, 11, 1232.
- [118] a) J. Wang, Z. Wei, S. Mao, H. Li, Y. Wang, *Energy Environ. Sci.* **2018**, 11, 800; b) Z. W. Seh, J. Kibsgaard, C. F. Dickens, I. Chorkendorff, J. K. Nørskov, T. F. Jaramillo, *Science* **2017**, 355, eaad4998.
- [119] L. Hui, Y. Xue, F. He, D. Jia, Y. Li, *Nano Energy* **2019**, 55, 135.
- [120] a) Y. Huan, J. Shi, X. Zou, Y. Gong, Z. Zhang, M. Li, L. Zhao, R. Xu, S. Jiang, X. Zhou, M. Hong, C. Xie, H. Li, X. Lang, Q. Zhang, L. Gu, X. Yan, Y. Zhang, *Adv. Mater.* **2018**, 30, 1705916; b) Z. Zhu, H. Yin, C. T. He, M. Al-Mamun, P. Liu, L. Jiang, Y. Zhao, Y. Wang, H. G. Yang, Z. Tang, D. Wang, X. M. Chen, H. Zhao, *Adv. Mater.* **2018**, 30, 1801171; c) C. Hu, L. Zhang, Z. J. Zhao, A. Li, X. Chang, J. Gong, *Adv. Mater.* **2018**, 30, 1705538; d) T. Yoon, K. S. Kim, *Adv. Funct. Mater.* **2016**, 26, 7386; e) Z. Wu, J. Wang, R. Liu, K. Xia, C. Xuan, J. Guo, W. Lei, D. Wang, *Nano Energy* **2017**, 32, 511; f) T. N. Ye, L. B. Lv, M. Xu, B. Zhang, K. X. Wang, J. Su, X. H. Li, J. S. Chen, *Nano Energy* **2015**, 15, 335; g) J. Jiang, M. Gao, W. Sheng, Y. Yan, *Angew. Chem., Int. Ed.* **2016**, 55, 15240; h) M. A. R. Anjum, H. Y. Jeong, M. H. Lee, H. S. Shin, J. S. Lee, *Adv. Mater.* **2018**, 30, 1707105.
- [121] Y. Xue, Y. Guo, Y. Yi, Y. Li, H. Liu, D. Li, W. Yang, Y. Li, *Nano Energy* **2016**, 30, 858.
- [122] a) X. Meng, L. Yu, C. Ma, B. Nan, R. Si, Y. Tu, J. Deng, D. Deng, X. Bao, *Nano Energy* **2019**, 61, 611; b) X. Huang, X. Xu, C. Li, D. Wu, D. Cheng, D. Cao, *Adv. Energy Mater.* **2019**, 9, 1803970; c) M. Kim, M. A. R. Anjum, M. Lee, B. J. Lee, J. S. Lee, *Adv. Funct. Mater.* **2019**, 29, 1809151; d) S. Li, C. Cheng, A. Sagaltchik, P. Pachfule, C. Zhao, A. Thomas, *Adv. Funct. Mater.* **2019**, 29, 1807419; e) Z. Li, C. Yu, Y. Wen, Y. Gao, X. Xing, Z. Wei, H. Sun, Y. W. Zhang, W. Song, *ACS Catal.* **2019**, 9, 5084; f) L. Li, Z. Qin, L. Ries, S. Hong, T. Michel, J. Yang, C. Salameh, M. Bechelany, P. Miele, D. Kaplan, M. Chhowalla, D. Voiry, *ACS Nano* **2019**, 13, 6824; g) A. Manikandan, P. R. Ilango, C. W. Chen, Y. C. Wang, Y. C. Shih, L. Lee, Z. M. Wang, H. Ko, Y.-L. Chueh, *J. Mater. Chem. A* **2018**, 6, 15320; h) Y. Zhou, J. V. Pondick, J. L. Silva, J. M. Woods, D. J. Hynek, G. Matthews, X. Shen, Q. Feng, W. Liu, Z. Lu, Z. Liang, B. Brena, S. Cai, M. Wu, L. Jiao, S. Hu, H. Wang, C. M. Araujo, J. J. Cha, *Small* **2019**, 15, 1900078.
- [123] E. J. Popczun, J. R. McKone, C. G. Read, A. J. Biacchi, A. M. Wiltrout, N. S. Lewis, R. E. Schaak, *J. Am. Chem. Soc.* **2013**, 135, 9267.
- [124] a) D. Voiry, R. Fullon, J. Yang, E. S. C. de Carvalho Castro, R. Kappera, I. Bozkurt, D. Kaplan, M. J. Lagos, P. E. Batson, G. Gupta, A. D. Mohite, L. Dong, D. Er, V. B. Shenoy, T. Asefa, M. Chhowalla, *Nat. Mater.* **2016**, 15, 1003; b) D. Voiry, H. Yamaguchi, J. Li, R. Silva, D. C. Alves, T. Fujita, M. Chen, T. Asefa, V. B. Shenoy, G. Eda, M. Chhowalla, *Nat. Mater.* **2013**, 12, 850; c) H. Yin, S. Zhao, K. Zhao, A. Muqsit, H. Tang, L. Chang, H. Zhao, Y. Gao, Z. Tang, *Nat. Commun.* **2015**, 6, 6430.
- [125] Q. Wang, M. Nakabayashi, T. Hisatomi, S. Sun, S. Akiyama, Z. Wang, Z. Pan, X. Xiao, T. Yamada, N. Shibata, T. Takata, K. Domen, *Nat. Mater.* **2019**, 18, 827.
- [126] S. Zhao, Y. Wang, J. Dong, C. T. He, H. Yin, P. An, K. Zhao, X. Zhang, C. Gao, L. Zhang, J. Lv, J. Wang, J. Zhang, A. M. Khattak, N. A. Khan, Z. Wei, J. Zhang, S. Liu, H. Zhao, Z. Tang, *Nat. Energy* **2016**, 1, 16184.
- [127] M. Chen, L. Wang, H. Yang, S. Zhao, H. Xu, G. Wu, *J. Power Sources* **2018**, 375, 277.
- [128] J. Yang, Y. Xiao, Q. Zhao, G. Zhang, R. Wang, G. Teng, X. Chen, M. Weng, D. He, S. Mu, Y. Lin, F. Pan, *Nano Energy* **2019**, 59, 443.
- [129] H. Huang, F. Li, Y. Zhang, Y. Chen, *J. Mater. Chem. A* **2019**, 7, 5575.
- [130] H. Y. Si, C. J. Mao, J. Y. Zhou, X. F. Rong, Q. X. Deng, S. L. Chen, J. J. Zhao, X. G. Sun, Y. M. Shen, W. J. Feng, P. Gao, J. Zhang, *Carbon* **2018**, 132, 598.
- [131] Z. Chen, W. Gong, Z. Liu, S. Cong, Z. Zheng, Z. Wang, W. Zhang, J. Ma, H. Yu, G. Li, W. Lu, W. Ren, Z. Zhao, *Nano Energy* **2019**, 60, 394.
- [132] Y. Wang, Y. Li, T. Heine, *J. Am. Chem. Soc.* **2018**, 140, 12732.
- [133] H. Zhang, W. Zhou, T. Chen, B. Y. Guan, Z. Li, X. W. Lou, *Energy Environ. Sci.* **2018**, 11, 1980.
- [134] Y. Gao, Z. Cai, X. Wu, Z. Lv, P. Wu, C. Cai, *ACS Catal.* **2018**, 8, 10364.
- [135] Y. Li, *Int. J. Electrochem. Sci.* **2018**, 13, 12226.
- [136] a) J. Lin, P. Wang, H. Wang, C. Li, X. Si, J. Qi, J. Cao, Z. Zhong, W. Fei, J. Feng, *Adv. Sci.* **2019**, 6, 1900246; b) P. W. Menezes, A. Indra, I. Zaharieva, C. Walter, S. Loos, S. Hoffmann, R. Schlögl, H. Dau, M. Driess, *Energy Environ. Sci.* **2019**, 12, 988; c) Y. Zhang, K. Rui, Z. Ma, W. Sun, Q. Wang, P. Wu, Q. Zhang, D. Li, M. Du, W. Zhang, H. Lin, J. Zhu, *Chem. Mater.* **2018**, 30, 4762; d) Z. Wang, Y. Inoue, T. Hisatomi, R. Ishikawa, Q. Wang, T. Takata, S. Chen, N. Shibata, Y. Ikuhara, K. Domen, *Nat. Catal.* **2018**, 1, 756.
- [137] E. Hu, Y. Feng, J. Nai, D. Zhao, Y. Hu, X. W. Lou, *Energy Environ. Sci.* **2018**, 11, 872.
- [138] Y. Xue, Z. Zuo, Y. Li, H. Liu, Y. Li, *Small* **2017**, 13, 1700936.
- [139] a) X. Wang, W. Li, D. Xiong, D. Y. Petrovykh, L. Liu, *Adv. Funct. Mater.* **2016**, 26, 4067; b) B. Bayatsarmadi, Y. Zheng, Y. Tang, M. Jaroniec, S. Z. Qiao, *Small* **2016**, 12, 3703; c) H. Huang, C. Yu, J. Yang, C. Zhao, X. Han, Z. Liu, J. Qiu, *ChemElectroChem* **2016**, 3, 719; d) K. Qu, Y. Zheng, Y. Jiao, X. Zhang, S. Dai, S. Z. Qiao, *Adv. Energy Mater.* **2017**, 7, 1602068; e) Y. Hou, Z. Wen, S. Cui, S. Ci, S. Mao, J. Chen, *Adv. Funct. Mater.* **2015**, 25, 872; f) D. Das, K. K. Nanda, *Nano Energy* **2016**, 30, 303; g) X. Zhang, S. Liu, Y. Zang, R. Liu, G. Liu, G. Wang, Y. Zhang, H. Zhang, H. Zhao, *Nano Energy* **2016**, 30, 93.
- [140] L. Yu, I. K. Mishra, Y. Xie, H. Zhou, J. Sun, J. Zhou, Y. Ni, D. Luo, F. Yu, Y. Yu, S. Chen, Z. Ren, *Nano Energy* **2018**, 53, 492.
- [141] a) C. Ling, L. Q. Zhou, H. Jia, *RSC Adv.* **2014**, 4, 24692; b) I. C. Man, H. Y. Su, F. Calle-Vallejo, H. A. Hansen, J. I. Martínez, N. G. Inoglu, J. Kitchin, T. F. Jaramillo, J. K. Nørskov, J. Rossmeisl, *ChemCatChem* **2011**, 3, 1159.
- [142] Y. Gu, S. Chen, J. Ren, Y. A. Jia, C. Chen, S. Komarneni, D. Yang, X. Yao, *ACS Nano* **2018**, 12, 245.
- [143] Z. Dai, H. Geng, J. Wang, Y. Luo, B. Li, Y. Zong, J. Yang, Y. Guo, Y. Zheng, X. Wang, Q. Yan, *ACS Nano* **2017**, 11, 11031.
- [144] P. W. Menezes, C. Panda, S. Garai, C. Walter, A. Guet, M. Driess, *Angew. Chem., Int. Ed.* **2018**, 57, 15237.
- [145] F. Luo, Q. Zhang, X. Yu, S. Xiao, Y. Ling, H. Hu, L. Guo, Z. Yang, L. Huang, W. Cai, H. Cheng, *Angew. Chem., Int. Ed.* **2018**, 57, 14862.
- [146] B. You, N. Jiang, M. Sheng, S. Gul, J. Yano, Y. Sun, *Chem. Mater.* **2015**, 27, 7636.
- [147] R. Lin, H. Lei, D. Ruan, K. Jiang, X. Yu, Z. Wang, W. Mai, H. Yan, *Nano Energy* **2019**, 56, 82.
- [148] M. Zhu, Q. Shao, Y. Qian, X. Huang, *Nano Energy* **2019**, 56, 330.
- [149] Z. Yuan, J. Li, M. Yang, Z. Fang, J. Jian, D. Yu, X. Chen, L. Dai, *J. Am. Chem. Soc.* **2019**, 141, 4972.
- [150] R. Yang, Y. Zhou, Y. Xing, D. Li, D. Jiang, M. Chen, W. Shi, S. Yuan, *Appl. Catal., B* **2019**, 253, 131.

- [151] P. Guo, J. Wu, X.-B. Li, J. Luo, W.-M. Lau, H. Liu, X. L. Sun, L. M. Liu, *Nano Energy* **2018**, 47, 96.
- [152] H. Yan, Y. Xie, A. Wu, Z. Cai, L. Wang, C. Tian, X. Zhang, H. Fu, *Adv. Mater.* **2019**, 31, 1901174.
- [153] L. An, J. Feng, Y. Zhang, R. Wang, H. Liu, G. C. Wang, F. Cheng, P. Xi, *Adv. Funct. Mater.* **2019**, 29, 1805298.
- [154] Y. Sun, K. Xu, Z. Wei, H. Li, T. Zhang, X. Li, W. Cai, J. Ma, H. J. Fan, Y. Li, *Adv. Mater.* **2018**, 30, 1802121.
- [155] Y. Xiong, L. Xu, C. Jin, Q. Sun, *Appl. Catal., B* **2019**, 254, 329.
- [156] Y. Hou, M. Qiu, T. Zhang, X. Zhuang, C. S. Kim, C. Yuan, X. Feng, *Adv. Mater.* **2017**, 29, 1701589.
- [157] a) H. Cheng, L. X. Ding, G. F. Chen, L. Zhang, J. Xue, H. Wang, *Adv. Mater.* **2018**, 30, 1803694; b) H. Liu, L. Wei, F. Liu, Z. Pei, J. Shi, Z. j. Wang, D. He, Y. Chen, *ACS Catal.* **2019**, 9, 5245.
- [158] W. Qiu, X. Y. Xie, J. Qiu, W. H. Fang, R. Liang, X. Ren, X. Ji, G. Cui, A. M. Asiri, G. Cui, B. Tang, X. Sun, *Nat. Commun.* **2018**, 9, 3485.
- [159] K. Ithisuphalap, H. Zhang, L. Guo, Q. Yang, H. Yang, G. Wu, *Small Methods* **2019**, 3, 1800352.
- [160] L. Hu, A. Khaniya, J. Wang, G. Chen, W. E. Kaden, X. Feng, *ACS Catal.* **2018**, 8, 9312.
- [161] a) M. M. Shi, D. Bao, B. R. Wulan, Y. H. Li, Y. F. Zhang, J. M. Yan, Q. Jiang, *Adv. Mater.* **2017**, 29, 1606550; b) J. Deng, J. A. Iñiguez, C. Liu, *Joule* **2018**, 2, 846; c) S. J. Li, D. Bao, M. M. Shi, B. R. Wulan, J. M. Yan, Q. Jiang, *Adv. Mater.* **2017**, 29, 1700001.